Alma Mater Studiorum - Università di Bologna

DOTTORATO DI RICERCA IN

ONCOLOGIA, EMATOLOGIA E PATOLOGIA

Ciclo 34

Settore Concorsuale: 06/I1 - DIAGNOSTICA PER IMMAGINI, RADIOTERAPIA E NEURORADIOLOGIA

Settore Scientifico Disciplinare: MED/36 - DIAGNOSTICA PER IMMAGINI E RADIOTERAPIA

MAGNETIC RESONANCE IMAGING-DERIVED BIOMARKERS OF ISOCITRATE-DEHYDROGENASE MUTATION IN DIFFUSE GLIOMAS: A CONVENTIONAL MR AND DIFFUSION-WEIGHTED IMAGING STUDY

Presentata da: Paola Feraco

Coordinatore Dottorato

Manuela Ferracin

Supervisore

Alessio Giuseppe Morganti

Esame finale anno 2022

-

A Te Papà, per la sete di conoscenza,
l'amore e l'offerta di TE.

INDEX

INTRODUCTION

The introduction of molecular criteria into the classification of diffuse gliomas has given rise to interesting, wide-ranging implications regarding glioma management [1-2]. Indeed, since 2016, in the World Health Organization (WHO) classification of Tumors of the Central Nervous System (CNS) [1-2], molecular parameters have been integrated with histopathology into gliomas characterization, creating more biologically homogenous groups.

In particular, all diffuse gliomas have been grouped based on the mutational state of the gene that codes for Isocitrate dehydrogenase (IDH) in its isoforms (IDH1 and IDH2) [1-2].

The integrated use of phenotypic and genotypic parameters permits the definition of more homogeneous diagnostic categories with greater objectivity than in the past. Thus, it will consequently be possible to establish more precise correlations between prognosis and response to the treatment of such neoplasms. In particular, IDH-Wilde Type (WT) astrocytomas exhibit a worse prognosis when compared with IDH-Mutant (MUT) [3]. Thus, the mutational status characterization might lead to new approaches for better overall patient management.

In particular, a non-invasive method that provides an accurate pre-surgical diagnosis has the potential to improve patient treatment planning from the initial presentation. For example, the knowledge that a tumour is an IDH-MUT glioma would favour a more aggressive surgical resection, as recent studies suggest that a greater extent of resection independently correlates with survival in IDH-mutant astrocytic gliomas [4].

The analysis of histopathological specimens through immunohistochemistry and genomic sequence is the gold standard method for detecting IDH mutations in patients with glioma. However, these methods are

invasive, and standard biopsies may lead to incorrect results due to intra-tumoral heterogeneity. Moreover, some tumours cannot be resectable since they are located in an eloquent critical area. On the other hand, medical imaging procedures can evaluate the entire tumour in a non-invasive and reproducible way.

Thus, a new clinical need has arisen to correlate imaging characteristics with glioma genotypes, also known as *radiogenomics or imaging genomics*. Whilst many studies have primarily focused recently on the use of advanced MRI techniques (perfusion, spectroscopy, and machine learning techniques) for radiogenomics purposes [5-7], conventional MRI sequences still remain the reference point in the study and characterization of brain tumours. Moreover, since it remains a challenge to standardise post-processing methods regarding advanced techniques and computational imaging approaches (such as machine learning), the utility of a study on conventional imaging features of glioma molecular subtypes should be useful as a tool for daily diagnostic brain tumour management.

Most of the literature on this topic has been published in the last five years, it is continuously growing, and to date, a restricted number of studies have been published.

Moreover, a different approach may rely on diffusion-weighted imaging (DWI) usage, which is considered a “conventional” sequence in line with recently published directions on glioma imaging [8]. In a non-invasive way, it can provide direct insight into the microscopic physical properties of tissues. Indeed, DWI, evaluating the Brownian movement of water molecules, indirectly reflects cellularity within the lesions through apparent diffusion coefficient (ADC) values [9]. ADC measures the magnitude of the random motion of water molecules within a tissue, and it is calculated by using data from DWI pulse sequences.

It has been widely described that ADC maps provide information about tissue microarchitecture. In particular, significant inverse correlations between ADC, cell count, and ki67 have been reported [10,11].

Considering that IDH gene mutations may reflect alterations in metabolism, cellularity, and angiogenesis, which may manifest characteristic features on an MRI [12–14], the identification of specific MRI biomarkers could be of great interest in managing patients with brain gliomas.

My study aimed to evaluate the presence of specific MRI-derived biomarkers of IDH molecular status through conventional MRI and DWI sequences.

GLIOMA WHO CLASSIFICATION

In the current revised 2021 WHO classification, all diffuse gliomas (of astrocytic origin and non-astrocytic origin) have been grouped together based on: their growth pattern, clinical behaviour, and specifically the sharing of the mutational state of the gene that codes for IDH in its isoforms (IDH1 and IDH2) [1-2].

CNS tumour grading has traditionally been based exclusively on histological features, but specific molecular markers can now provide robust prognostic information. For this reason, molecular parameters have now been added as biomarkers also of grading and for further estimating prognosis within multiple tumour types. These molecular parameters currently constitute a crucial component of glioma diagnosis, providing a combined phenotypic and genotypic diagnosis.

All diffuse gliomas have been divided into *IDH-MUT* glioma and *IDH-WT*. In particular, diffuse astrocytic tumours IDH-MUT are considered a single type (*Astrocytoma, IDH -Mut*) and are then graded as CNS WHO grade 2, 3, or 4.

On the other hand, low-grade diffuse gliomas (grades 2 and 3) without an IDH mutation are known as *IDH-WT*, and they can be considered as "*molecular GBM*" [15,16].

IDH-MUT GBMs are not more recognized since they arise from low-grade gliomas and are now considered grade 4 IDH-MUT astrocytomas.

While the traditional grading system has failed to stratify the risk of IDH-MUT astrocytoma, canonical histological and proliferative markers may apply to the risk stratification of IDH-WT astrocytoma. Numerous studies have examined molecular markers to obtain more clinically relevant information that will improve the risk stratification of gliomas.

The 2021 WHO Classification of Tumors of the CNS adopted these molecular markers into the revised grading criteria of IDH-MUT and -WT astrocytoma, respectively, as a grading system within tumor types.

In particular, the *CDKN2A/B* homozygous deletion for IDH-MUT astrocytoma and the following three criteria for IDH-WT astrocytoma: the concurrent gain of whole chromosome 7 and loss of whole chromosome 10, *TERT* promoter mutations, and *EGFR* amplification, were identified as independent molecular markers of the worst clinical outcomes. The presence of *CDKN2A/B* homozygous deletion in an IDH-MUT tumor results in a CNS WHO grade of 4, even in the absence of microvascular proliferation or necrosis. In other words, a molecular parameter can sometimes add value to histological findings in assigning a grade [2].

While TERT promoter mutation, EGFR amplification, and +7/−10 copy number changes in IDH-wildtype diffuse astrocytomas allowing a IDH-WT CNS WHO grade 4 (GBM) designation even in cases that otherwise appear histologically lower grade (Figure 1).

Therefore, the revised classification incorporates these three genetic parameters as criteria for a diagnosis of GBM, IDH-WT. As a result, GBM IDH-WT should be diagnosed in the setting of an IDH-WT diffuse and astrocytic glioma in adults if there is microvascular proliferation or necrosis or TERT promoter mutation or EGFR gene amplification or +7/−10 chromosome copy number changes.

According to the current classification, the diagnosis of oligodendroglioma and anaplastic oligodendroglioma require the concomitant deletion of the short arm of chromosome 1 and the long arm of chromosome 19 (1p/19q co-deletion); this is in addition to the demonstration of the IDH mutation.

This genotypic feature is due to an unbalanced translocation between chromosome 1 and chromosome 19, and it is a powerful predictor of both

responses to therapy and survival [17]. Therefore, its presence must be ascertained in all tumors with oligodendroglial differentiation.

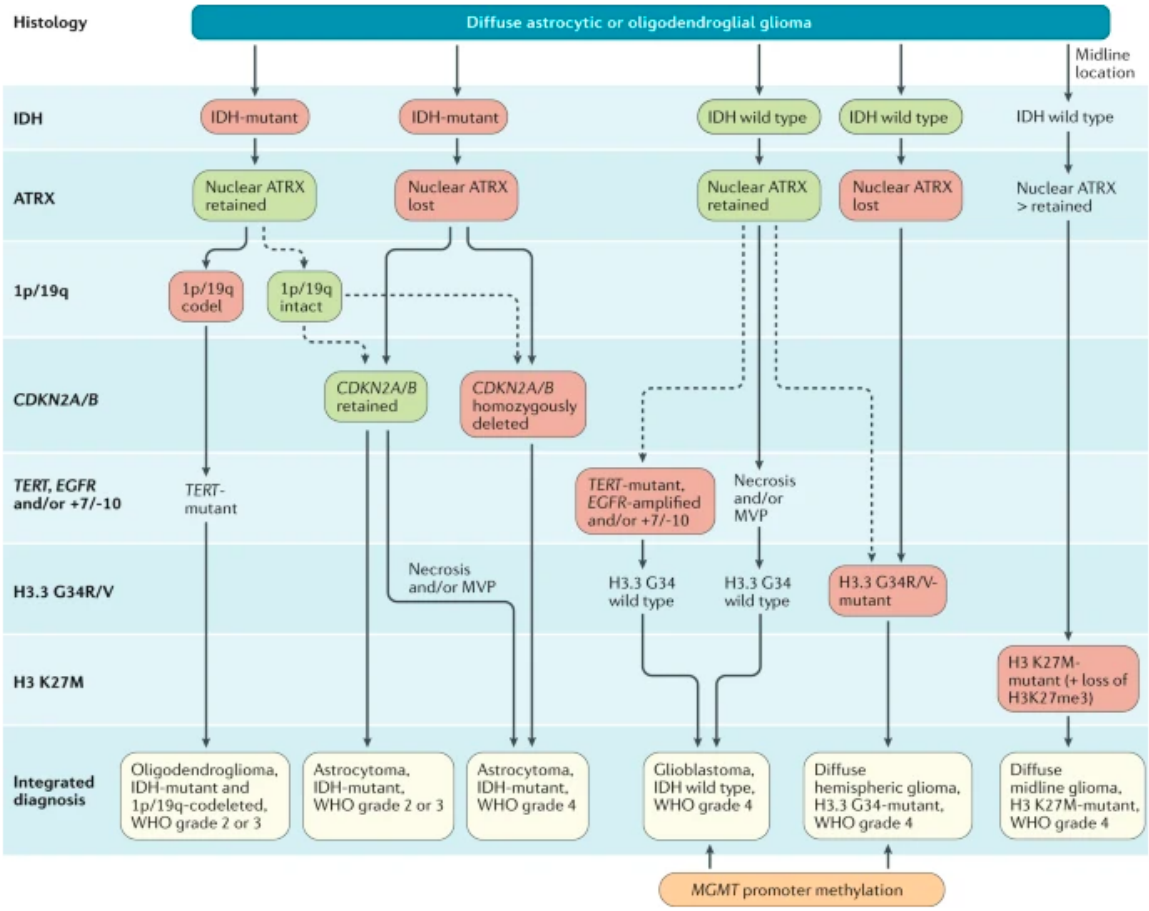

Fig 1: Diagnostic algorithm for the integrated classification of the major diffuse gliomas in adults. *From Weller M et al Nature Reviews Clinical Oncology* **volume 18**, pages170–186 (2021)

Isocitrate dehydrogenase

IDH enzymes, of which there are three isoforms, are essential enzymes that participate in several major metabolic processes, such as the Krebs cycle, glutamine metabolism, lipogenesis, and redox regulation [18]. IDH1 is located in the cytoplasm and peroxisomes, whereas IDH2 and IDH3 are located in the mitochondrial matrix. The catalytic sites of IDH1 and IDH2 exhibit affinity for the substrate, Isocitrate, together with nicotinamide adenine dinucleotide phosphate (NADP+) and a divalent metal cation,

resulting in the formation of α-ketoglutarate (α-KG) (Figure 2). IDH3, which also catalyses the transformation from Isocitrate into α-KG, employs nicotinamide adenine dinucleotide (NAD+) as its cofactor [19]. The catalytic activity of IDH requires homodimerization and an alteration in the enzyme conformation; Isocitrate binding changes the structure of the enzyme from an open to a closed conformation. Substrate recognition depends on the amino acid residues in the active site, whereas the frequent mutated active site residue in cancer is arginine 132 (R132) [20].

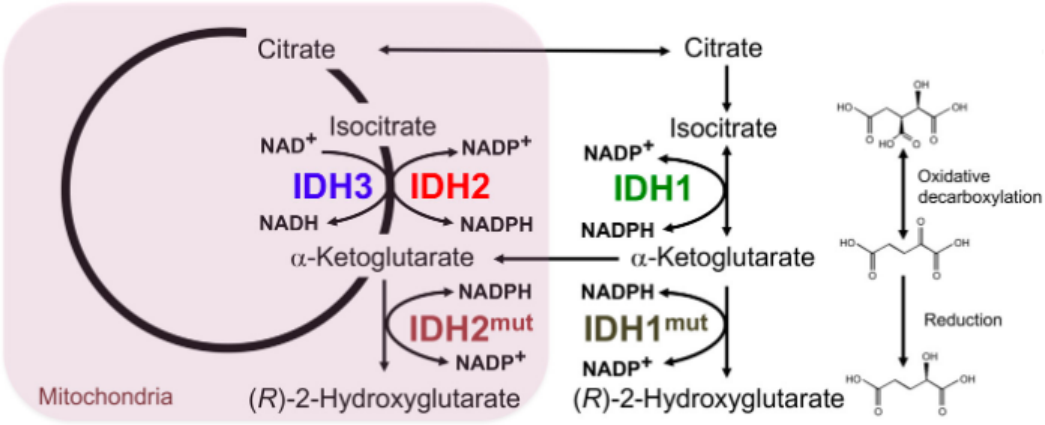

Fig 2 Subcellular localization and chemical reactions catalyzed by wild-type IDH and tumor-derived IDH mutant enzymes.

Isocitrate dehydrogenase mutation

Mutations in IDH are prevalent in human malignancies. Mutations of the IDH gene family produce oncometabolite 2- hydroxyglutarate (2-HG), leading to slower growth of tumour cells than the wild types [21]. In glioma, IDH mutations are recognized in >80% of WHO grade 2/3 cases. IDH mutations have been shown to be one of the earliest glioma formation events.

The resulting production of 2HG appears to drive extensive epigenetic changes that alter cellular differentiation and could contribute to oncogenesis (Figure 3).

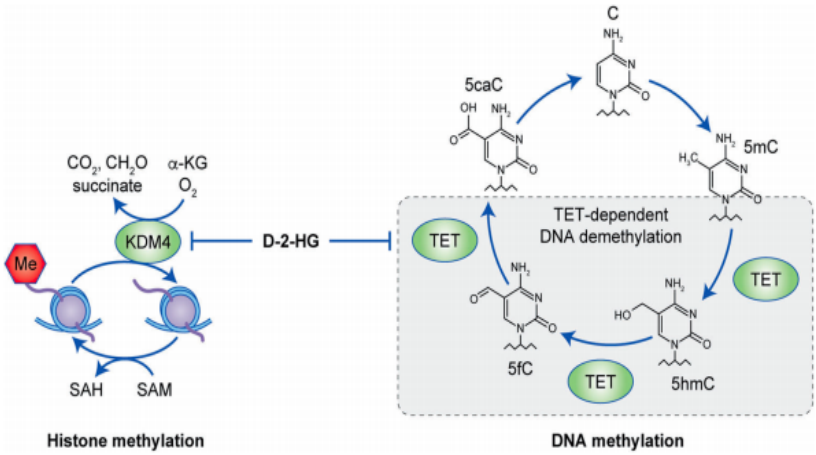

Fig 3. IDH Mutants result in alteration throughout the epigenome. Owing to structural similarity, IDH1-mutant-derived D-2-HG serves as a competitive inhibitor for KDM4 or TET and therefore blocks the demethylation process in histone and nucleotide, respectively.

Although IDH-mutated glioma generally exhibits a better disease outcome, the high incidence of IDH mutations in secondary GBM (now Astrocytoma grade 4) suggests that lower-grade glioma with IDH mutation often recur with having undergone a malignant transformation to a higher grade. In addition, IDH-mutated glioma is more likely to develop a hypermutation phenotype, which is associated with worsened prognosis [22].

IDH mutations associated with cancer tend to localize to the arginine residue, which is crucial for recognizing Isocitrate (R132 for IDH1, R140, or R172 for IDH2) [23]. Missense mutations in the IDH1 gene result in the replacement of a strong, positively charged arginine residue at position 132 with lower polarity amino acids such as histidine (H), lysine (K) or cysteine (C), which impedes the formation of hydrogen bonds with the αcarboxyl and β-carboxyl sites of Isocitrate. Therefore, the mutant IDH enzyme exhibits decreased affinity for Isocitrate, along with an elevated preference for NADPH. However, only one copy of the IDH gene is mutated in tumours, and in tumour cells harbouring heterozygous IDH mutations, the primary forms of IDH

dimers are presumed to be heterodimers that contain a version of wild-type IDH1 and a version with the R132H mutation. As a result, in IDH-mutant cells, the IDH1 wild-type component of the dimer converts Isocitrate into α-KG to produce NADPH. In contrast, the mutant part of the dimer exhibits neo-morphic activity, converting α-KG into D-2-hydroxyglutarate (D-2-HG) in an NADPH-dependent manner [24].

The first phase in glioma molecular characterization is *IDH testing* regardless of grade.

An Immunohistochemical investigation of the most frequent IDH1 mutation (R132H) should be routinely performed on all tissue samples where diffuse glioma is suspected (Figure 4). This is primarily because the test can be decisive in the differential diagnosis between infiltrating astrocytoma and reactive gliosis [25-27].

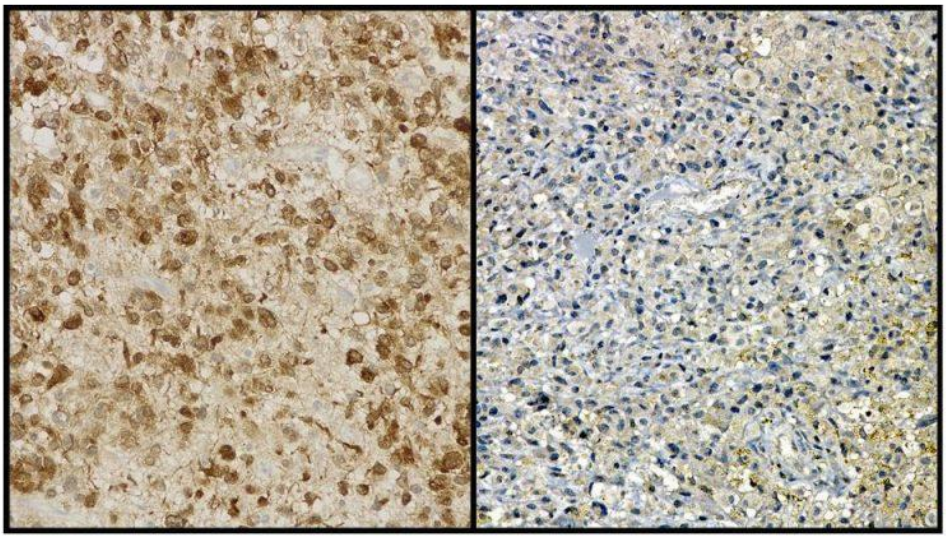

Fig 4 Example of an Immunohistochemical investigation in IDH mutant and IDH wild type gliomas. Mutant IDH1(R132H)- specific immunohistochemistry showing immunoreactivity for IDH1 mutant protein in infiltrating tumour cells (on the left), supporting the diagnosis of IDH1-mutant glioma. No immunoreactivity for IDH1 (on the right side) in a WT glioma.

DIAGNOSTIC APPROACH TO DIFFUSE GLIOMA

In consideration of its intrinsic multiparametric characteristics and of the various "functional" techniques available, MRI represents, to date, the reference point in the study and characterization of brain tumours. In particular, conventional MRI is invaluable for glioma genotyping, particularly regarding tumours, which are presumed to be lower grade.

In general, low-grade gliomas are homogeneously hypointense in T1w and hyperintense on T2w, with little or no expansive effect; high-grade tumours, on the other hand, have an inhomogeneous signal (due to the presence of microcalcifications, necrotic-cystic or hemorrhagic areas), poorly defined and irregular margins, are surrounded by perilesional edema and exert an evident expansive effect on adjacent structures. The administration of a paramagnetic contrast medium based on gadolinium chelates adds further diagnostic information; the presence of contrast enhancement is associated with high-grade gliomas, but it should be emphasised that it is not always suggestive of high histological degree (pilocytic astrocytoma and pleomorphic xanthoastrocytoma are low-grade tumours that present intense contrast enhancement) and, conversely, about 1/3 of high-grade tumours do not show contrast enhancement.

Imaging plays a vital role in diagnosing and managing patients with brain glioma. The modern techniques of MR, with both morphological and functional studies, allow characterising different diagnostic aspects, from the extension of the disease to the histopathological grading, necessary for the planning of surgical therapy. An MRI is the primary non-invasive modality of choice for the early diagnostic work-up of gliomas. Various MRI advanced techniques, such as DWI, perfusion-weighted imaging (PWI), and proton magnetic resonance spectroscopy (1H-MRS), have also been applied to detect the IDH mutation status [5-7]. Moreover, susceptibility-weighted imaging

(SWI), and dynamic susceptibility contrast perfusion-weighted imaging (DSC-PWI) are non-invasive techniques for genetic subtypes classification of gliomas [12,28]. SWI has been used for assessing tumour vascularity and blood products by intratumoral susceptibility signals (ITSSs) [29,30].
Regarding IDH mutation, 1H-MRS can directly detect the presence of 2-HG and the consequent IDH mutational status. On the other hand, this technique is usually limited to the academic world, and conventional MRI sequences remain the reference point in studying and characterising brain tumours.

Diffusion Weighted Imaging

In addition to basic MRI protocols, DWI has been routinely performed in MRI glioma protocols [8], and nowadays, it might be considered a conventional sequence.
DWI can non-invasively reflect tumour cellularity and extracellular space through the measurement of apparent diffusion coefficient (ADC) values. Here we describe the basis of this useful technique.

Technique

DWI is an MRI technique sensitive to the Brownian motion of water molecules, spontaneous and constant movement induced by the thermal kinetic energy of the molecules themselves [31].
In a container of water, the thermal movement of the single molecules is free from constraints or restrictions, and the molecular diffusion is therefore described as a stochastic (random and, therefore, probabilistic) and isotropic (equal and constant in all directions of space) physical phenomenon in which the spatial dislocation of the molecules follows a logic of the Gaussian type [32]. In this case, the diffusion can be quantitatively described by the diffusion coefficient "D" of Einstein's equation, who was the first to demonstrate how microscopic molecular motion could be explained using Fick's laws on

macroscopic diffusion phenomena according to gradient [33]. However, in biological tissues, the diffusion of water molecules is not free; instead, it is limited and constrained by multiple interactions with various macromolecular structures such as proteins, fibers, or cell membranes. Therefore, the diffusive motion loses the isotropy that would occur in a glass of pure water, while the spatial distribution of the molecules, observable in a given time interval, stops obeying the Gaussian distribution laws; in these cases, the diffusion model offered by Einstein is no longer adequate to describe the complexity of the phenomenon observed, making it necessary to introduce the so-called "apparent diffusion coefficient" (ADC), a term used to describe the influence of multiple factors on a movement no longer simply driven by thermal agitation and concentration gradients [31,32,34]. Precisely, the observable diffusion in biological tissues consists of various molecular motions that coincide with the different aqueous compartments of the organism, namely intra-cellular, extracellular and intravascular. It goes without saying that any pathophysiological process that alters the volumetric ratios between the compartments mentioned above, or the physical integrity of the macromolecular barriers (such as cell membranes), will affect the diffusion of water molecules and, therefore, the characteristics of the signal obtained in DWI acquisitions, making this method a highly informative tool of the functional architecture of a tissue [31-34].

From a technical point of view, the weighting of the diffusion MR image is based on a spin-echo sequence modified by the addition of two equal and opposite gradients applied before and after the 180 ° refocus pulse (Figure 5). Applying the first field gradient along a spatial axis induces a loss of phase coherence of the spins of the water molecules, with consequent attenuation of the transverse magnetization. In the case of stationary spins, applying the second gradient involves a complete recovery of the transverse magnetization as if the gradients had never been applied. On the other hand, in the case of

spin in motion, the application of the second gradient does not allow to compensate for the offset induced by the first adequately. In this way, a net loss of the transverse magnetization is obtained, resulting in an attenuation of the echo signal and indirect index diffusion of water molecules in the tissue. The magnitude of the observed signal drop is proportional to the extension of the molecular movement and to the properties of the diffusion gradients used (amplitude, duration, and time elapsed between the application of the two gradients), enclosed in the parameter called "b-value." In particular, the b-value is an operator-dependent parameter that indicates the extent of the diffusion weighting of the acquired image. As the value of this parameter increases, the contrast between tissue components with different diffusion increases exponentially, but at the same time, the global signal strength decays.

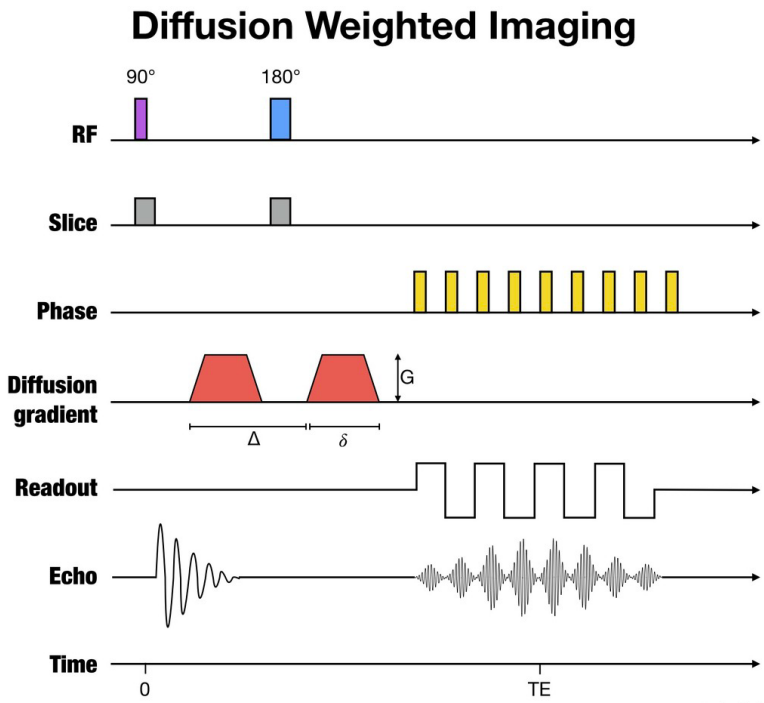

Fig 5 Schematic representation of a DWI sequence (Case courtesy of A.Prof Frank Gaillard, Radiopaedia.org, rID: 21753)

The extension of the molecular movement measurable in vivo is instead represented by the apparent diffusion coefficient (ADC): it is a direct index of the speed with which the loss of signal occurs between two or more acquisitions at different b-values and measures the area covered by the stochastic movement of water molecules in the unit of time. Values of ADCs can be obtained pixel-by-pixel and represented on a mono-parametric map automatically generated in the post-processing phase, which allows a quantitative evaluation of diffusion phenomena through the selection of regions of interest (ROI) [31-34]. The measurement of ADC values is commonly used to evaluate multiple pathological processes, especially in the oncological field, since the variation of the water content and diffusibility within a tumour lesion and in the adjacent tissues provides information otherwise not obtainable through the conventional MR imaging. In general, in high cell density neoplasms, there is an increased representation of the aqueous intra-cellular space at the expense of the extracellular one, with a restriction of the diffusion of water molecules. In these cases, the signal will appear relatively conserved as the b-value increases, with relatively low ADC values compared to healthy tissue.

On the other hand, a disintegration of cell membranes in intrinsically necrotic tumours or after effective therapy is reflected in an increase in the extracellular space at the expense of the intracellular space, with a greater diffusion of water molecules: in this case, the signal reduction observed with increasing b-value is more conspicuous and rapid, with relatively higher ADC values compared to densely cellular tissue [35, 36] (Figure 6).

Different correlations between ADC and various histological properties (such as tumour proliferation index, tumour grade, and presence of necrosis) have demonstrated the validity of the DWI technique in providing a potential biomarker imaging in the characterization of tumours in vivo, both

concerning neoplasms cerebral [37] and extra-cranial oncological pathology [38].

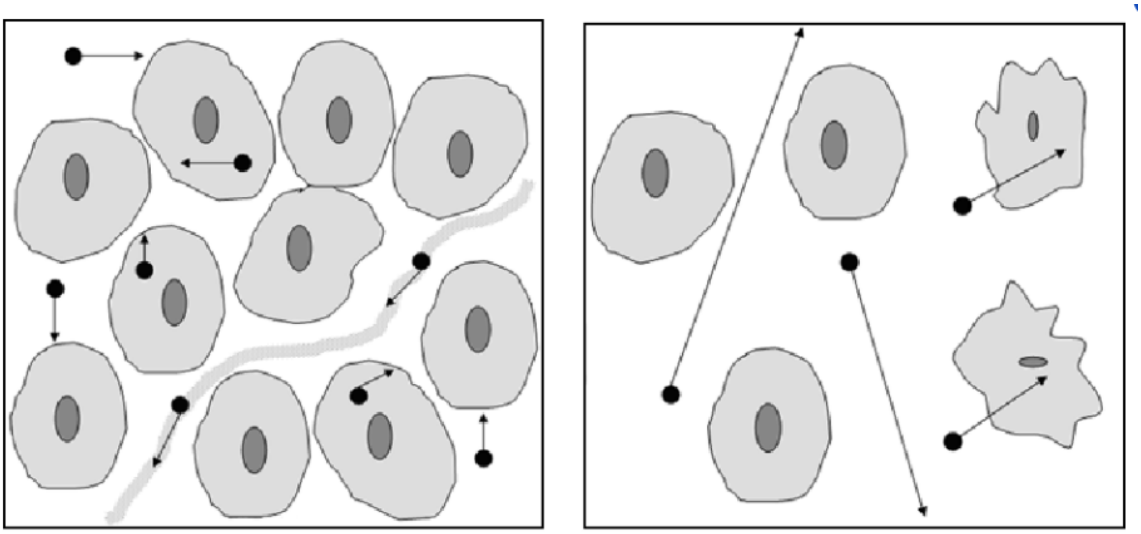

A B

Fig. 6—Diffusion of water molecules. A, Restricted diffusion: cellularity and intact cell membranes. Drawing represents 1 voxel of tissue evaluated by diffusion-weighted imaging (DWI) containing cells and blood vessels. Note water molecules (black circles with arrows) within extracellular space, intracellular space, and intravascular space, all of which contribute to measured MR signal. In this highly cellular environment, water diffusion is restricted because of reduced extracellular space and by cell membranes, which act as a barrier to water movement. B, Free diffusion: low cellularity and defective cell membranes. In a less cellular environment, relative increase in extracellular space allows freer water diffusion than more cellular environment would. Defective cell membranes also allow movement of water molecules between extracellular and intracellular spaces

PROJECT

Purpose

Considering that IDH gene mutations may reflect alterations in metabolism, cellularity, and angiogenesis, which may manifest characteristic features on an MRI [12-14], the identification of specific MRI features could be of great interest in managing patients with brain gliomas.

Moreover, recently, some studies have shown that ADC maps may easily discriminate the IDH mutations status, although most of them did not consider homogeneous groups of gliomas in terms of grading and histology [39–43]. Indeed, ADC can be influenced by histology and grading [44–47].

This study aimed to evaluate the presence of specific MRI-derived biomarkers of IDH molecular status through conventional MRI and DWI sequences, focusing on grade 2 and 3 astrocytic and oligodendroglial tumours. Moreover, we wanted to define the prognostic impact of MRI parameters and what might be the best predictive MRI-derived biomarker of OS.

Materials and Methods

Patient Cohort

This multicentre retrospective study was approved by the Human Research Ethics Committee of the "*Azienda Provinciale per i Servizi Sanitari* (APSS)" of Trento *(*Prot—MOLIMA—07 Mar 2019*)* and *Area Vasta Bologna* (Prot 604/2019/OSS/AUSLBO). Written informed consent was obtained from all participants.

Two-hundred fifty-eight (258) adult patients with newly diagnosed supratentorial intra-axial brain tumours who underwent surgical resection or stereotactic biopsy at our institutions from July 2013 through October 2019 were selected.

The inclusion criteria were:

- ✔ availability of the IDH mutation status and/or 1p/19q status;
- ✔ pre-surgical or pre-chemo-radiotherapy MRI and DWI images.
- ✔ Immunohistochemical antibody testing for IDH1-R132H mutation;

Patients were excluded in cases of a lack of pre-surgical or pre-chemo/radiotherapy treatment imaging.
For imaging analyses, we focused on WHO grades 2 and 3 gliomas with the following histologic diagnosis:

- ✔ Astrocytoma;
- ✔ Oligodendroglioma;
- ✔ Oligoastrocytoma;
- ✔ Diffuse glioma;

Pathology and Immunohistochemical Analysis

The nature and grade of the gliomas were determined according to the 2016 WHO classification [1]. IDH mutational status was determined by Immunohistochemical antibody testing for the IDH1-R132H mutation, the most common glioma-derived mutation. Among IDH1-MUT, to exclude patients with concomitant 1p/19q co-deletion and, thus, a diagnosis of oligodendroglioma, fluorescence in-situ hybridization was performed. The methods for these molecular analyses have been described elsewhere [48,49].

MR Imaging Acquisition

MRI studies were performed on three magnets (two 1.5 Tesla and one 3 Tesla; Intera Achieva; Philips, Best, the Netherlands and Magnetom Avanto;

Siemens, Enlargen, Germany; g.e. Discovery Optima MRI 450). All patients received routine clinical MRI scans, including pre-contrast Spin Echo (SE) T1-weighted images and Fluid Attenuation Inversion Recovery (FLAIR) and Turbo Spin Echo (TSE) T2-weighted images, acquired at least in the axial plane. Following gadolinium compound bolus administration (0.1 mmol/kg, macrocyclic ionic agent), at least an axial SE T1-weighted or a 3D T1-weighted Fast Field Echo (FFE) sequence was acquired. These sequences were performed with variable section thickness ranging from 1 to 4 mm.

T2*-based MR imaging, including either conventional T2* gradient echo (GRE) sequences or susceptibility-weighted imaging (SWI), was performed in 68 patients. On each scanner, the DWI acquisition consisted of a diffusion-sensitised axial 2D spin-echo sequence with EPI readout, with two b values of 0 and 1000 s/mm2. Section thickness ranged from 3 to 4 mm, with interslice gaps of 0–1 mm. Diffusion gradients were applied in the x, y, and z directions. ADC maps were automatically calculated by the integrated scanner software and converted into standard units (10−3 mm2/s).

Imaging Analysis

Conventional imaging evaluation

Two European board-certified neuroradiologists assessed all images with more than 15 years of experience blinded to the pathological diagnosis. MR imaging features included: (1) tumour location (frontal, parietal, temporal, insular or occipital); (2) hemisphere (right, left or bilateral); (3) signal intensity on T2w (homogeneous/heterogeneous); (4) well-defined borders on FLAIR images (yes/no); T2/FLAIR mismatch sign (presence vs. absence); (5) peritumoral edema on T2/FLAIR images (presence vs. absence) and (6) contrast enhancement presence (yes/no).

DWI analysis

Images were analysed on a dedicated off-line workstation (Advantage Workstation 4.3_8 GE) using the provided analysis software (Functool, version 9.4.05a, GE Healthcare Systems).

The placement of the region of interests (ROIs) was performed as previously described by Xing Z. et al. [40]. In particular, to ensure precise ROIs placements on the solid tumour components and avoid cystic, hemorrhagic, and necrotic areas or peritumoral edema, the DWI images were co-registered with conventional MRI (FSE T1w pre-gadolinium and 3D FSPGR post-gadolinium and T2w FRFSE). Hence, the mean ADC values (ADCm) were measured by manually placing ROIs on the ADC maps (elliptical ROIs of approximately 15–30 mm2). From three to five non-overlapping ROIs were placed inside the visually lowest ADC tumour areas (Figure 7).

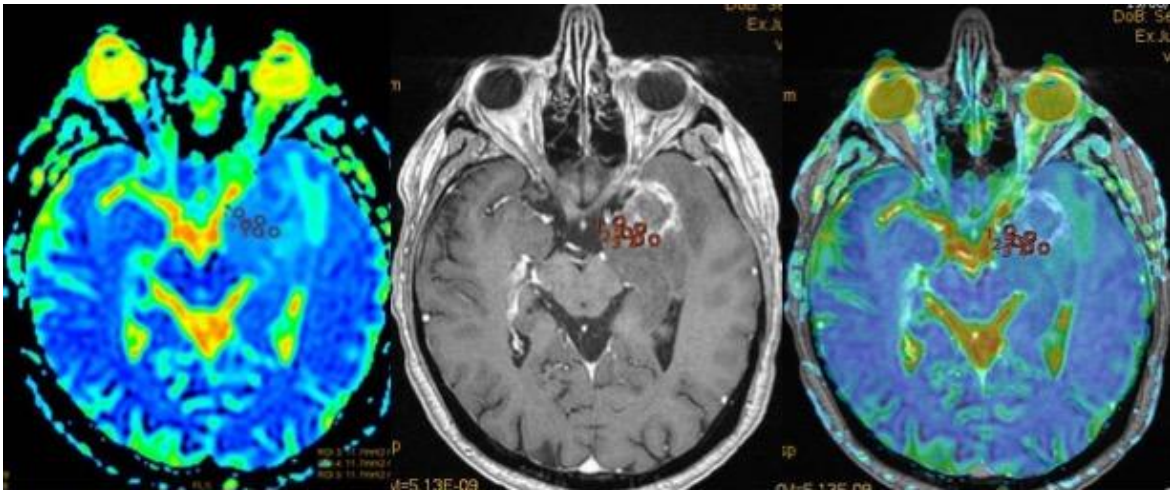

Fig 7 Placement of region on interests (ROIs) on the apparent diffusion coefficient (ADC) map: (a) co-registration between T1-weighted and colour-coded ADC map (blue: restricted diffusion; red: facilitated diffusion); (b) placement of five elliptical ROIs on parametric ADC map within the tumour. Co-registration allows identification of the different components of the tumour and peritumoral region.

Eventually, to minimise variances in ADCm values, relative ADC (rADCm) was obtained from the ratios of the tumour ADCm to the ADCm of a normal-appearing reference region (left cerebellum), defined on T2-weighted and contrast-enhanced T1-weighted images (CE-T1w). Moreover, the lowest ADCm and rADCm values were chosen for each patient.

Statistical analysis

Statistical analyses were performed using the "R" [50]. Descriptive statistics included mean, minimum, and standard deviation of continuous variables and scores; in the case of categorical parameters, numbers and percentages distributions were used.

ANOVA and Tukey's *t*-test were used respectively to evaluate the quantitative differences (ADCm and rADCm) among groups (IDH-MUT, IDH-WT, and IDH-MUT 1p/19q co-deleted).

Fisher's exact test was used to evaluate qualitative (borders, enhancement, edema, T2w signal, T2/Flair mismatch sign) prevalence in each IDH group. The agreement between the two raters was estimated using Cohen's kappa statistics.

A multinomial logistic regression model was performed to determine the ability of conventional MRI features and rADCm to discriminate the IDH mutational status. The sensitivity, specificity, positive predictive value, negative predictive value, and area under the curve based on optimum thresholds for variable parameters were calculated. OS in all groups was calculated with the Kaplan-Meier method. Comparison between survival curves was performed using the log-rank test.

A classification and regression tree (CART) analysis was then used to better identify the three groups in terms of ADC, T2w signal, and T2/FLAIR mismatch sign. Lastly, a multivariate analysis of OS as a function of IDH and MRI features using the proportional-hazard Cox regression model was

performed. This multivariate analysis makes it possible to evaluate the influence of "ceteris paribus" on the probability of OS of each of the factors, with the exact influence of the other factors considered. A $p<0.05$ was considered statistically significant for all the tests.

Literature research

To contextualise and compare our results with literature data, an extensive research in the English language literature was performed in September 2021 in PubMed (https://pubmed. ncbi.nlm.nih.gov, accessed on 10 September 2021), using the following keywords and their combinations: "diffuse glioma," "glioblastoma," "astrocytoma," "oligodendroglioma" AND "Isocitrate dehydrogenase," "IDH," "1p19q", AND "magnetic resonance imaging". Preclinical and clinical studies from the last five years (January 2016–September 2021) were carefully reviewed, focusing on the different diffuse glioma molecular subtypes. The publication date was restricted to the last five years since the latest update of WHO brain tumour classification was specified as given in 2016. Various articles within this time range were included to maximise this review's topic coverage. Where available, full texts in English were included, together with the most significant corresponding references.

The exclusion criteria were: unavailability of full text, non-English publications; case reports; Letters; commentaries; reviews; editorials; no interpretation of conventional MRI (cMRI) sequences; studies limited to advanced MR sequences or machine learning, and studies devoid of glioma molecular subtype information. Conventional MRI findings were described from the included studies, after which they were systematically organised and grouped according to a particular field of study and perspective.

Results

From the overall patient's sample screened (n = 248), 142 tumours that underwent surgery were GBM. As a result, 114 patients, 83 astrocytic, (39 G2 and 44 G3) and 31 oligodendroglial tumours were included in the study (M:75, F:39).

Demographic characteristics and conventional MRI features of the molecular subgroups in the astrocytic group are shown in Table 1.

Demographic results

Regarding age, a significant difference was found between the subgroups. Patients with the IDH mutation were younger than those not mutated ($p < 0.001$) (Figure 8). In particular, based on the multiple post-hoc comparisons between the pairs of means (Tukey test), there is a statistically significant difference between IDH-MUT and IDH-WT (p-value 0.0003), between IDH-MUT 1p/19q-codeleted and IDH-WT (p-value = 0.009); while there is no statistically significant difference between IDH-MUT 1p/19q-codeleted and IDH-MUT 1p/19q- not-co-deleted (p-value = 0.873)

Concerning sex, although a male prevalence in the astrocytic group has been found in the general population ($p<0.001$), no significant differences were found comparing IDH groups.

Table 1. The main clinical and MRI features of the patient sample are divided according to IDH mutational status in grade 2 and 3 gliomas.

	IDH MUT (50)	**IDH WT (33pt)**	**IDH MUT-cod(31)**	***p*-Value**
Age	41 ± 14,5	54 ± 13,3	43±13,3	***0.0003***
Location				0.08
Frontal lobe	**29 (58)**	12(36)	18 (56)	
Temporal lobe	11(22)	13(39)	6(18)	
Insular	2 (4)	3(18)	6(18)	
Other	8 (16)	5(15)	2(6)	
T2w Signal Intensity				***0.0004***
Homogeneous	23(65)	12(35)	0	
Heterogeneous	7(20)	*20 (58)*	7(20)	
Cystic	*20(54)*	1(2)	16(43)	
Calcification	0	0	*9(100)*	
Borders				***0.0000***
Defined	30***(79)***	8(21)	0	
Indistinct	20(26)	25(32)	32(41)	
Edema				0.05
Yes	30(62)	21(64)	28(87)	
No	19(38)	12(36)	4(13)	
Contrast enhancement				
Yes	13(26)	15(27)	21***(42)***	***0.001***
No	37***(56)***	18(30)	11(16)	
T2/Flair mismatch				***0.0000***
Yes	33 (***100***)	0	0	
No	17(21)	33(40)	31(38)	
T2* ITSS	0-1	0-1	0-3	***0.007***
rADCm values	1,90	1,43	1,57	***0.0001***
Standard deviation	±0,381	±0,297	±0,256	

The numbers in parentheses represent the percentages of the total number of each group.

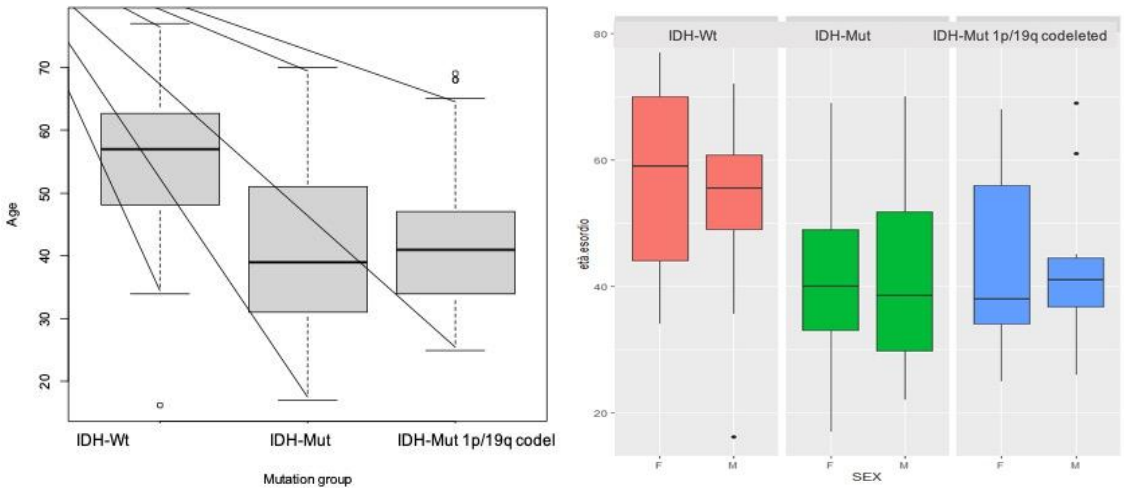

(a) **(b)**

Fig 8 Boxplots showing age (a) and sex (b) of Mutational groups. Patients with IDH-MUT and IDH-MUT 1p/19q co-deleted tumour are younger than those not mutated (difference significant for $p < 0.001$). No significant prevalence was found in sex distribution in each groups.

Conventional MRI results

The typical characteristics of IDH-MUT and IDH-WT tumours are shown in Figures 9,10 and 11. Tumours with IDH mutation were located mainly in the frontal (58%) and temporal (22%) lobes, such as those with 1p/19q co-deletion, while there was no significant location prevalence in the WT group.

Concerning borders, there was a significant difference between groups; indeed, IDH-WT and IDH-MUT 1p/19q co-deleted had a significant prevalence of ill-defined borders if compared with the IDH-MUT group, which has a predominance of sharp borders (p=0.00).

Regarding T2w signal intensity, IDH-MUT 1p/19q-codeleted were all inhomogeneous with cystic and/or calcific components, IDH-MUT were prevalently homogeneous and cystic and IDH-WT both heterogeneous and homogeneous with significant differences among groups (p<0.001). In the T2* images, the groups were significantly different in the amount of ITSS; indeed, IDH-MUT didn't show significant ITSS if compared with IDH-WT and IDH-MUT 1p/19q co-deleted (p<0.001).

T2/Flair mismatch sign was observed in 33 out 50 IDH-MUT 1p/19q not co-deleted tumours (87%) but was not seen in any of 33 *IDH-Wt* astrocytomas nor in 31 IDH-MUT 1p/19q co-deleted (p=0.00). The sensitivity, specificity, PPV, NPV, and accuracy of T2/FLAIR mismatch in predicting *IDH*-MUT astrocytomas were 66%, 100%, 100%, 79.4%, and 60%, respectively. The interrater agreement for the T2/FLAIR mismatch-positivity in *IDH*-MUT astrocytomas was excellent (*K=1*).

Concerning contrast enhancement (C.E.), IDH-MUT 1p/19q co-deleted exhibited significant C.E. if compared with other groups (P<0.001). While no significant differences were found between IDH-MUT and IDH-WT, IDH-MUT showed less C.E. if compared with IDH-WT.

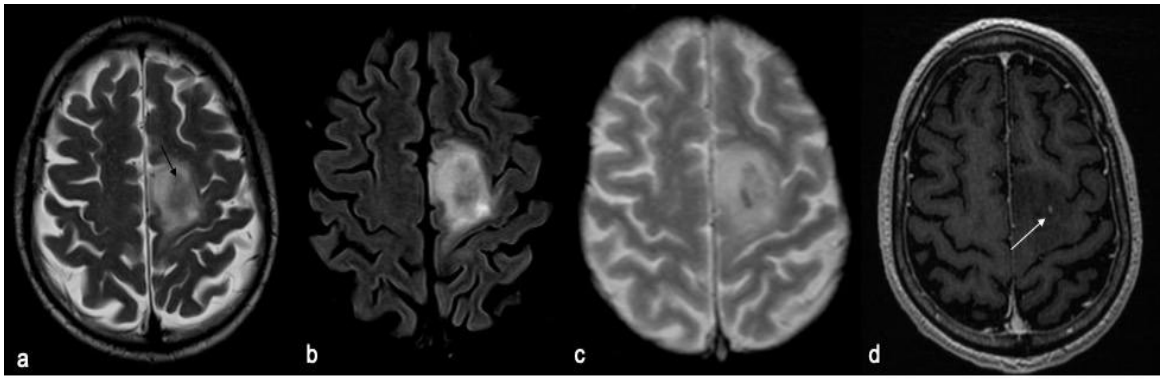

Fig 9 MRI characteristics of diffuse glioma IDH-MUT 1p/19q co-delated (oligodendroglioma grade 2). T2w fast spin echo (a), T2w FLAIR (b), T2*-weighted gradient echo (c) and T1w fast spin echo contrast-enhanced (c) images are shown. Mesial frontal mass with low mass effect and without any significant enhancement after contrast (arrow in c indicate the only spot of blood-brain barrier leakage), and some intra-tumoral calcifications (arrow in a; CT not shown) with no T2/FLAIR mismatch sign.

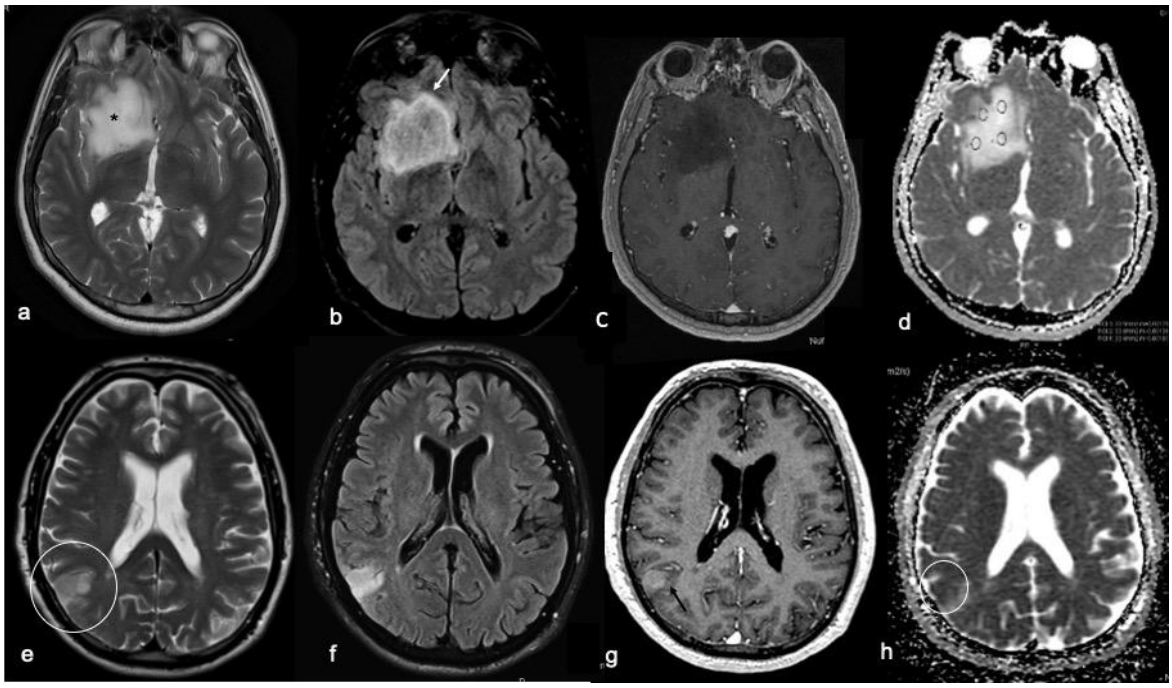

Fig 10 Conventional MRI characteristics of grade 3 IDH-MUT (top row: a-d) and IDH-WT (bottom row: e-h) diffuse gliomas. For each case, T2w fast spin echo (a, e), FLAIR sequences (b, f), T1w fast spin echo contrast-enhanced (c, g), and ADC map (d, h) images are shown. (a-d) Right frontal tumour with defined borders, high and homogeneous T2w signal (asterisk in a), T2w/FLAIR mismatch sign (arrow in b), no contrast enhancement and high ADC values; these are the typical imaging finding of an IDH-MUT glioma. (e-h) Right parietal ill-defined tumour (inside the circled in e) characterised by low T2w signal (e), no evidence of T2w/FLAIR mismatch sign (f), slight contrast enhancement (g) and low signal in ADC maps (h); these imaging finding are typical of an IDH-WT glioma.

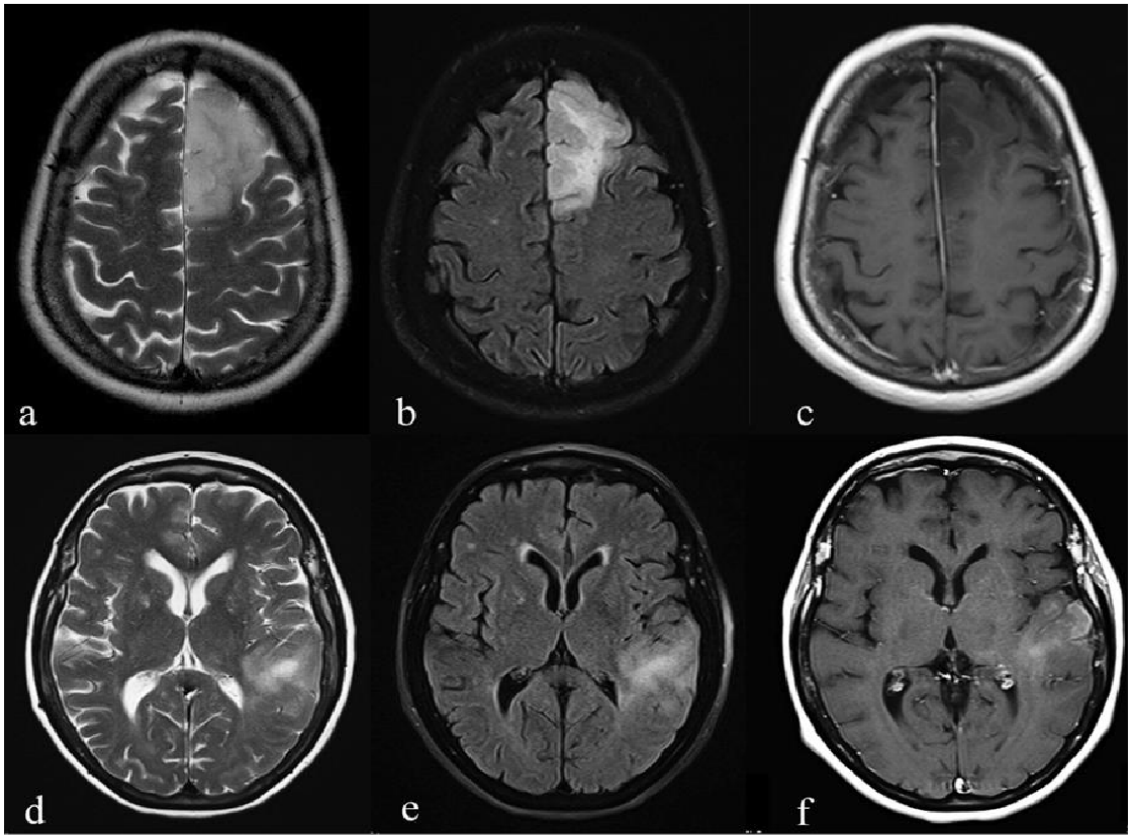

Fig 11. Pre-surgical conventional MR images of two patients with Grade III astrocytoma: (a–c) T2-weighted, fluid-attenuated inversion recovery images (FLAIR) and T1-weighted post-gadolinium images of an IDH-mutant (MUT) tumor show a lesion on the left frontal lobe. The borders are well-defined on T2-weighted (a) and FLAIR (b) images. No areas of T1-shortening are evident after IV contrast medium administration; (d–f) T2-weighted, FLAIR and T1-weighted post-gadolinium of an IDH-wild type (WT) tumor show a hyperintense T2-weighted (d) and FLAIR (e) lesion on the left temporal lobe. Ill-defined borders (d,e) and a blurred contrast enhancement are detected (f).

ADC and rADCm results

Regarding the DWI sequences, significant differences were found in ADCm and rADCm values between IDH-WT and IDH-MUT tumours of equal grade with higher values in the IDH-MUT compared to the IDH-WT group. It was also possible to distinguish oligodendroglioma from IDH-MUT (Fig 12). Indeed, the average rADCm of "WT" patients was 1.43; the average rADCm of "IDH-MUT" patients was 1.90, while the average rADCm of "IDH-MUT 1p/19 co-deleted" patients was 1.57. The difference between the means was statistically significant (ANOVA p-value=0). Based on the multiple post-hoc

comparisons between the pairs of means (Tukey test), there was a statistically significant difference between IDH-MUT and IDH-WT (p-value 0), between IDH-MUT and IDH-MUT 1p/19 co-deleted (p-value = 0.0008); while there was no statistically significant difference between IDH-MUT 1p/19 co-deleted and IDH-WT (p-value = 0.278).

ROC analysis indicated that ADCm and rADCm variables had similar diagnostic performances in differentiating the IDH-MUT vs. IDH-WT lesions. The value of ADCm 0.98x10-3 mm2/s and of rADCm of 1.44 emerged as a "cut-off" to differentiate the mutation state between IDH MUT and IDH-Wt.

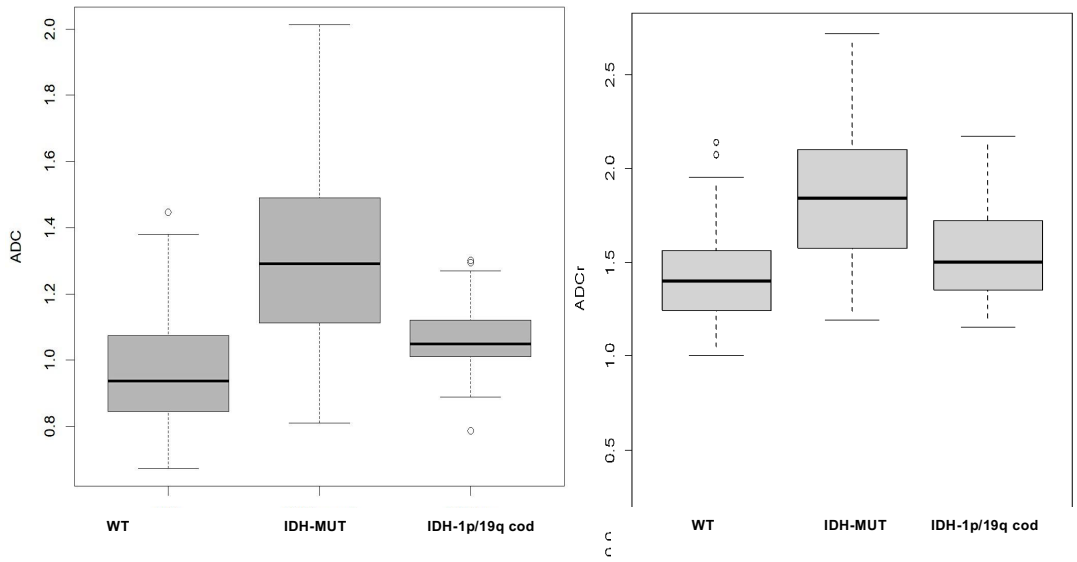

(a) **(b)**

Fig 12 Boxplots showing Differences in ADC (a) and rADCm (b) among IDH-WT, IDH-MUT and IDH-MUT 1p/19 co-deleted. A statistically significant difference between both the ADC and rADCm values of IDH-MUT and WT tumors (p-value 0) and between IDH-MUT and IDH-MUT 1p/19 co-deleted (p -value = 0.0002) has been found; while the difference between IDH-MUT 1p/19 co-deleted and WT is not significant.

In an attempt to identify which factors could better predict the IDH mutation and distinguish groups, different classification methods were applied (e.g., bi and multinomial logistic model and CART). The results of the ROC curve analysis are shown in Table 2.

	Cut-off (ADC)	Predicted class	Sensitivity	Specificity	PPV	NPV	AUC (95% CI)
ADC	0.989	WT	0.645	0.892	0.741	0.841	0.769 (0.675-0.862)
		MUT	0.907	0.434	0.565	0.852	0.671 (0.590-0.751)
		MUT_Codel	0.000	1.000	-	0.771	-
ADC + Mismatch	0.989	WT	0.645	0.906	0.769	0.841	0.776 (0.683-0.869)
		MUT	***0.651***	***1.000***	***1.000***	***0.776***	***0.826 (0.754-0.898)***
		MUT_Codel	0.857	0.689	0.439	0.944	0.773 (0.680-0.866)
ADC + Mismatch + T2	0.989	WT	0.645	0.906	0.769	0.841	0.776 (0.683-0.869)
		MUT	***0.767***	***0.923***	0.892	0.828	***0.845 (0.772-0.919)***
		MUT_Codel	***0.857***	***0.811***	0.563	0.952	***0.834 (0.745-0.923)***
ADC + Mismatch + T2*	0.989	WT	0.931	0.636	0.575	0.946	0.784 (0.704-0.863)
		MUT	0.694	1.000	1.000	0.814	0.847 (0.771-0.924)
		MUT_Codel	0.421	0.938	0.667	0.847	0.680 (0.562-0.798)
ADC + Mismatch + T2 + T2*	0.989	WT	0.759	0.836	0.710	0.868	0.798 (0.704-0.891)
		MUT	0.694	1.000	1.000	0.814	0.847 (0.771-0.924)
		MUT_Codel	0.842	0.815	0.571	0.946	0.829 (0.732-0.926)
ADC + Mismatch + T2 + T2* + enhan+border	0.989	WT	***0.793***	***0.855***	0.742	0.887	***0.824 (0.735-0.912)***
		MUT	***0.722***	***1.000***	1.000	0.828	***0.861 (0.787-0.935)***
		MUT_Codel	***0.895***	***0.846***	0.630	0.965	***0.870 (0.787-0.954)***

Table 2. Cut-off, sensitivity, specificity, PPV, NPV, and AUC of parameters for assessing the IDH and 1p/19q co-deletion status of grade 2 and 3 gliomas.

A combination of ADC and T2/Flair mismatch sign yielded good results for the diagnosis of IDH mutation status. In addition, the evaluation of T2w signal intensity together with ADC and T2/Flair mismatch provided good results for the diagnosis of both IDH-MUT and IDH-MUT 1p/19q co-deleted tumours. While a model also comprising cMRI features (enhancement and borders) provided good results for the identification of the overall groups.

Classification and regression tree (CART) analysis was also used to better predict the three (IDH-WT, IDH-MUT, and IDH-MUT 1p/19q co-deleted) and two (IDH-MUT and IDH-WT) groups (Figure 13) in terms of T2/Flair mismatch sign, T2w signal and rADCm cut-off value of 1.44. This model yielded a good accuracy (0.76) for the three groups, which increased significantly (0.89) if we evaluated only IDH-MUT and IDH-WT tumors.

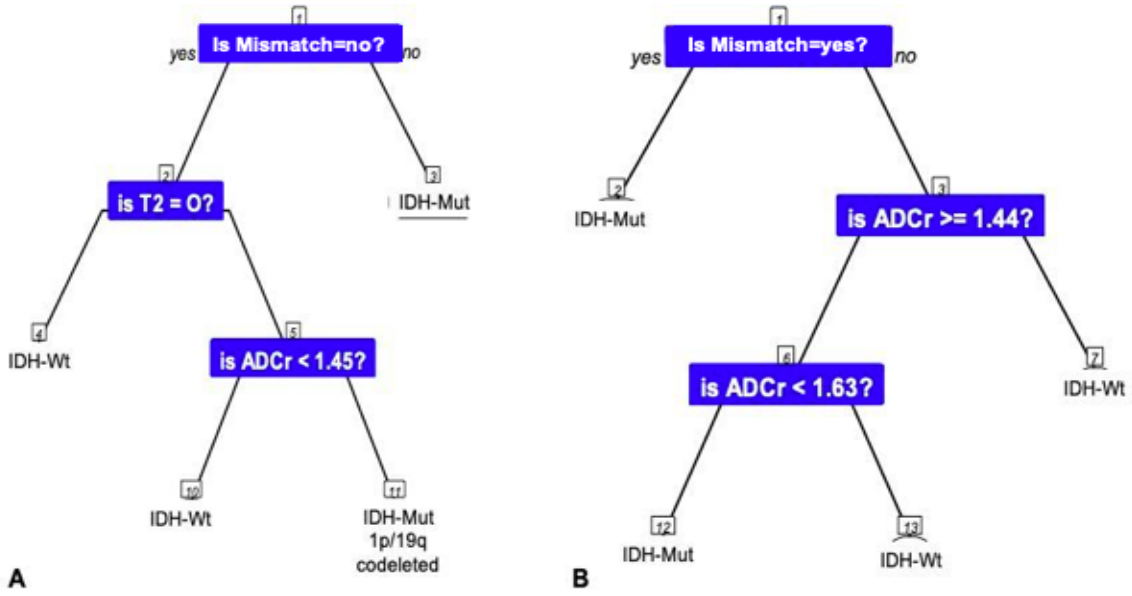

CONFUSION MATRIX (A)

Prediction	WT	IDH-MUT	1/19q cod
WT	32	8	6
IDH-MUT	0	35	5
1p/19q cod	1	7	21

Accuracy*: **0.7652*** / 95% CI : (0.6771, 0.8392) / Kappa : 0.6463

	IDH-WT	IDH-MUT	1p/19q cod
Sensitivity	**0.9697**	0.7000	0.6562
Specificity	**0.8293**	**0.9231**	**0.9036**
PPV	0.6957	0.8750	0.7241
NPV	0.9855	0.8000	0.8721

CONFUSION MATRIX (B)

Prediction	MUT	WT
MUT	42	1
WT	8	32

Accuracy**: *0.8916*** / 95% CI : (0.8041, 0.9492) /Kappa : 0.7815

Sensitivity*:*	***0.8400***
Specificity:	***0.9697***
PPV:	0.9767
NPV:	0.8000

Fig 13 Classification and regression tree (CART) analysis used to better predict the IDH-WT, IDH-MUT and IDH-MUT 1p/19q co-deleted groups (A), and IDH-WT and IDH-MUT (B) in terms of ADC, T2w signal and T2/FLAIR mismatch sign. By using this classification methods, the three groups (A) can be predicted with a good accuracy *(0.76)* which significantly increase *(0.89)* if we consider only gliomas with astrocytic origin (B).

Results of survival analysis

Concerning survival data and predictors of OS: Significant differences between survival curves of the three groups regarding IDH, contrast enhancement, edema, and T2/flair mismatch sign have been found (Kaplan-Meier p-value=0). In particular, as widely described in the literature, IDH mutation is an independent predictor of high OS in diffuse glioma (Figure 14).

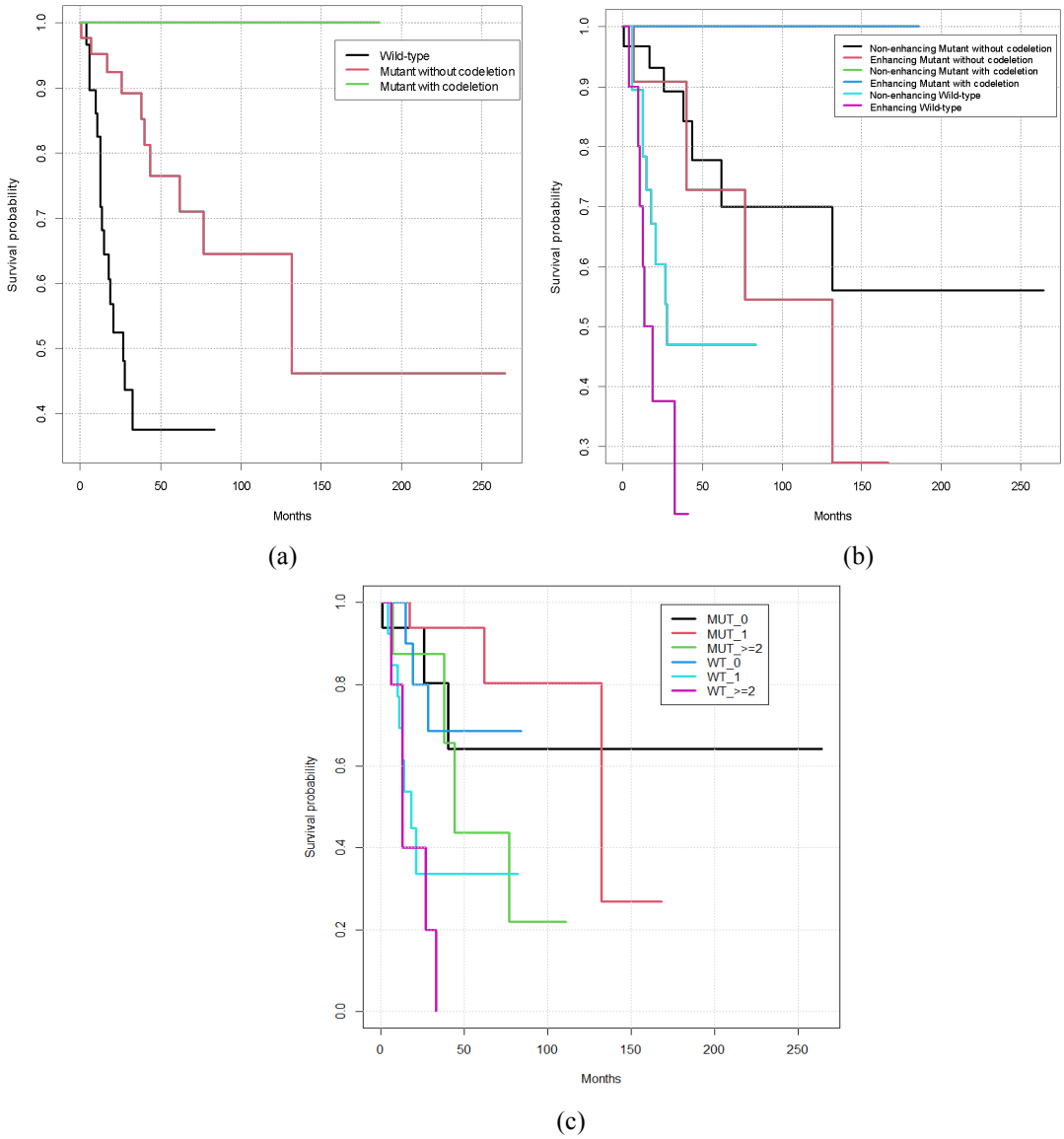

Fig 14 (a) Survival curves in mutational groups. Patients with ***IDH-mutation*** demonstrated significantly longer survival than WT (Kaplan-Meier test p-value 0). (b) Survival curves in mutational groups according to ***contrast enhancement***. Patients with IDH-mutation and no enhancement demonstrated significantly longer survival both in IDH-MUT and WT (Kaplan-Meier test p-value 0). (c) Survival curves in mutational groups according to ***edema rate*** (0, 1, >2). Patients without edema demonstrated significantly longer survival both in IDH-MUT and WT patients (Kaplan-Meier test p-value 0)

Among conventional MRI features, the presence of contrast enhancement and edema are negative prognostic factors both in IDH-WT and IDH-MUT tumours (P=0.00) (Figure 14), while the presence of T2/Flair mismatch sign emerged as a positive predictive factor of higher overall survival in IDH-MUT tumours (Figure 15).

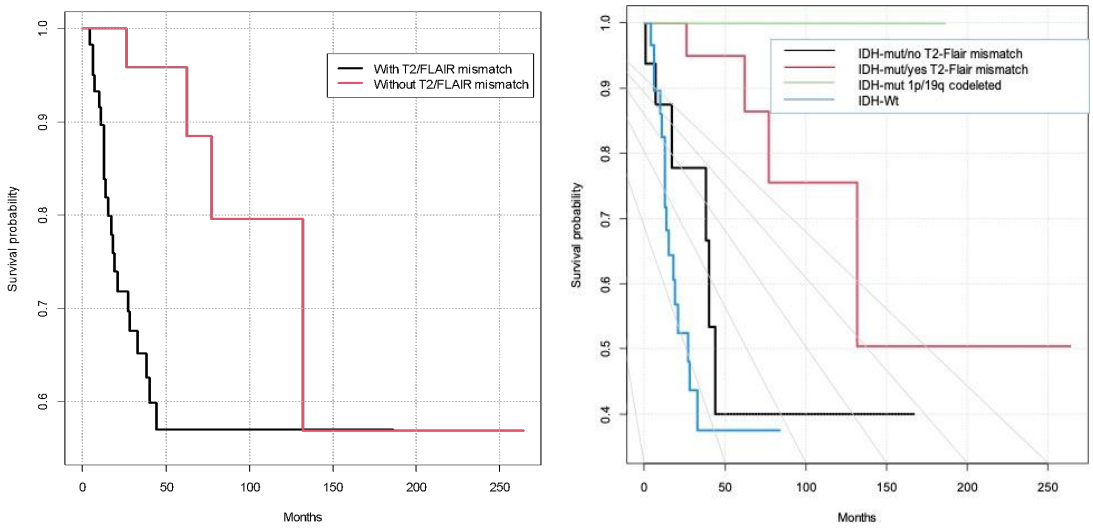

(a) (b)

Fig 15 Survival curves between combined mismatch and mutational groups. Patients with IDH-mutated lesions who had T2/Flair mismatch sign demonstrated significantly longer survival than WT and IDH-mutants who did not express T2/FLAIR mismatch sign (Kaplan-Meier test p-value 0).

Bibliographic results

One hundred and twenty-six articles were identified from the PubMed literature search. These were subsequently screened for relevance: 103 studies were excluded according to the exclusion criteria, while 23 were included. The full text was available for all of the 23 included studies, which were also included in the qualitative analysis. In the discussion, we grouped the MR findings regarding molecular subgroups, IDH and 1p/19q-codeletion, according to the principal reporting descriptive characteristics: location, borders, internal signal characteristics, contrast enhancement, T2w/FLAIR mismatch sign and diffusion-weighted imaging (DWI).

Discussion

In the current study, we explored whether conventional and diffusion MRI features could identify genetic subtypes of grade 2 and 3 gliomas. Our results showed that radiological characteristics, as visible on both conventional MRI and DWI, are significantly different between the three WHO 2016 gliomas subtypes (IDH-MUT, IDH-WT, and ODGs).

Considering the age and morphological features of our population, consistent with previous studies, younger age and a frontal location were more likely related to the mutational status, while older ages and no location prevalence to wild-type status [43,51]. The current hypothesis is that the IDH-MUT tumours arise from a neural precursor population with a defined spatial and temporal location [22,23]. Indeed, diffuse gliomas can be found in different locations, which reflect their tumour cell origin.

Different molecular subgroups have been demonstrated with a distinctive anatomic distribution, which is of great importance in patient diagnosis and clinical outcomes. This kind of anatomic feature is consistent with its corresponding histological subtypes. As in our patient sample, IDH-MUT tumours have been widely reported as being more frequently located in the frontal region compared to the temporo-insular region [43, 51] and also in the bilateral insular lobes [52]. Moreover, sub-ventricular zone involvement has also been related to IDH-MUT tumours [53]. In addition, tumours with the coexistence of IDH1 and telomerase reverse transcriptase (TERT) gene promoter mutations are inclined to grow in the left frontal lobe and close to the midline region. On the other hand, only TERT mutated glioma is more deeply located than IDH-MUT and 1p/19q co-deleted [52]. However, a non-lobar location and multifocal/multicentre distribution have been described as independent predictors of IDH-WT gliomas [54] (Figure 16).

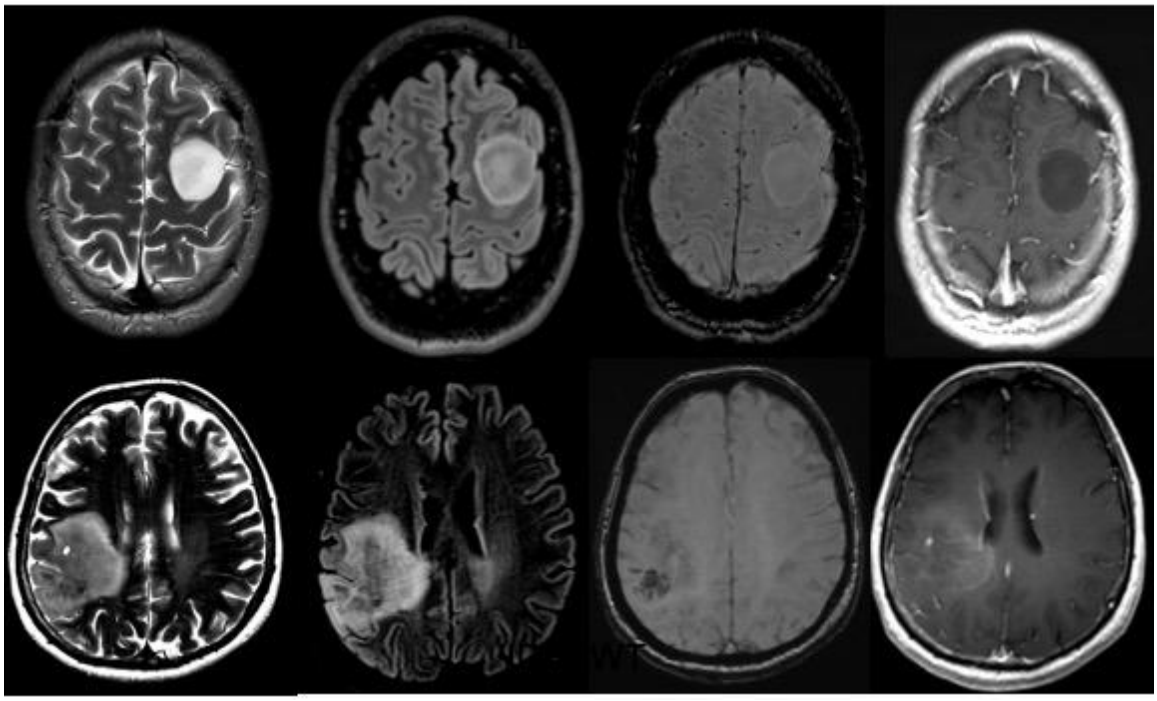

Fig 16 Conventional MRI characteristics of grade 3 IDH-MUT (top row) and IDH-WT (bottom row) diffuse gliomas. For each case, T2w fast spin echo, FLAIR sequences, T2*w SWI and T1w fast spin echo contrast-enhanced images are shown. At the top row, left frontal tumour with well-defined borders, high and homogeneous T2w signal, T2w/FLAIR mismatch sign no ITSS deposition on T2* images and no contrast enhancement; these are the typical imaging findings of an IDH-MUT glioma. On the bottom row, right parietal ill-defined tumour characterised by low T2w signal, no evidence of T2w/FLAIR mismatch sign, presence of ITSS on SWI images and slight contrast enhancement; these imaging finding are typical of an IDH-WT glioma.

Concerning borders, we found a strong significant relationship between defined borders and IDH-MUT status, while IDH-WT and –MUT 1p/19q co-deleted tumors had ill-delimited borders (p=0) predominantly. This result is consistent with the literature; in detail, an evaluation of borders on FLAIR images has enabled the discrimination between IDH-WT and IDH-MUT tumors, thereby demonstrating the ill-defined borders of IDH-WT [43] (Figure 16). Moreover, a poorly defined non-enhancing margin is an independent predictor of an IDH1-WT [54]. This data is an important characteristic regarding glioma management since border appearance is critical in defining surgery management, and knowledge of IDH status can also direct surgical planning.

Considering the T2w signal intensity characteristics, we found, as expected, significant differences among groups (p=0.0004). We found that a homogeneous and/or cystic T2w signal is significantly related to IDH-MUT 1p/19q intact tumour, while IDH-WT exhibited an inhomogeneous T2w signal may be due to the more necrotic composition of this kind of lesions [55]. The assessment of the tumours on T2w images may assist in making a differential diagnosis as described in the literature [54]. The evaluation of T2w images, and in particular the use of a quantitative approach through T2 mapping sequences, has recently shown that the T2 signal is significantly increased in IDH-MUT gliomas when compared to the wild type; this may be due to an accumulation of 2HG and modified tumour metabolism [56]. On the other hand, the presence of calcifications within IDH-MUT is typical of IDH-MUT 1p/19q co-deleted tumours [54], which bear a heterogeneous signal intensity in T2w images with a significantly higher micro-vascularity and higher vascular heterogeneity (Figure 9) [57]. Such tumours also show more pial invasion when compared with the IDH-MUT non co-deleted group [54].

Compared to 1p/19q-intact gliomas, 1p/19q-codeleted gliomas show a significantly lower rate of sharp borders and a higher rate of edema, heterogeneity, cysts, and calcification. In particular, high heterogeneity on T2w images and the presence of calcifications were predictive of 1p/19q co-deletion. Indeed, in our multinomial logistic model, adding the evaluation of the T2w parameter to ADC and T2/FLAIR mismatch sign helped in distinguishing IDH-MUT 1p/19q co-deleted tumours from the other two groups, making this simple sequence an easy tool for radiogenomics purpose.

Moreover, this kind of heterogeneity maybe is considered to be as a result of (micro) calcification, intratumoral haemorrhage, necrosis, and degeneration [54,55,57], which can be evaluated with the T2w and T2*w sequences. In particular, an evaluation of cerebral microbleeds through ITSS

in gliomas is of significant value in predicting the glioma grade, IDH1 mutation, and MGMT methylation. Indeed, IDH1-MUT and MGMT methylated tumours have significantly lower ITSS grades than gliomas IDH-WT and un-methylated MGMT [58]. But, although no relationship between 1p/19q deletion status and ITSS grades has yet been published, in our population, we found that a higher ITSS score is related to this mutational group.

Regarding contrast enhancement (C.E.), although we found a significant prevalence in C.E. only in IDH-MUT 1p/19q co-deleted tumours, a trend of higher enhancement on IDH-WT can be detected (see results table). Indeed, a larger proportion of enhancing tumours has been more frequently related to IDH-WT [54], indicating an unfavourable prognostic factor for this group [59]. Enhancement patterns in IDH-WT could be related to the molecular similarity of this subgroup with GBMs, which show a more infiltrative behaviour with blood barrier-disruption patterns on MRI.

Our data confirm that C.E. has been shown to be more frequent in IDH-MUT and 1p/19q co-deleted tumours [60] than in not-co-deleted IDH-MUT [61]. Indeed, after intravenous contrast administration, 1p/19q co-deleted tumours generally do not enhance. However, a patchy, multifocal enhancement with a dot-like or lacy pattern has been reported in up to 50% of cases [57]. This might assist in differentiating low-grade non co-delated IDH-MUT from 1p/19q co-deleted IDH-MUT.

The conventional MRI differences between IDH-MUT and IDH-WT in our opinion reflect the more aggressive biological behaviour of IDH-WT, as both C.E. and indistinct borders are seen more frequently in IDH-WT, and are believed to indicate invasiveness [62]. Moreover, we confirmed how the presence of C.E. is an adverse prognostic marker also in both WT and IDH-MUT tumours. Indeed, C.E. is another critical feature in exploring a possible brain tumour diagnosis and has been demonstrated as being associated with

OS [63]. Indeed, no enhancement and a smooth, non-enhancing margin, as revealed by MRI, are predictive of a longer PFS and OS in lower grade tumours [59,64].

Furthermore, sharp borders and frontal anatomical location typical of IDH-MUT may contribute to a better resectability, a larger extent of resection, and thus better survival.

Among conventional MRI data, our results showed that the T2/FLAIR mismatch sign represents a precise (100%) imaging biomarker for identifying IDH mutant gliomas 1p/19 not co-deleted, but with a low sensitivity (65.7%). This sign has been defined by the presence of two distinct MRI features as follows [65]:

1. Tumor displays the complete or near-complete and almost homogeneous hyperintense signal on T2-weighted images.
2. Tumor displays a relatively hypointense signal on the T2-weighted FLAIR sequence except for a hyperintense peripheral rim.

Moreover, the identification of this biomarker has been effective in differentiating gliomas with a better prognostic profile since IDH-MUT tumours which exhibited it had higher OS (see survival curves) if compared with IDH-MUT without T2/FLAIR mismatch sign. To our knowledge, no other relevant studies have been published on this result, which in our opinion, is worthy of further investigations to elucidate mechanisms and characteristics underlining the different survival behaviours between IDH-MUT groups.

In addition, T2/FLAIR mismatch sign constitutes an easily identifiable marker with a substantial agreement between more and less experienced radiologists (K=0.98%). Until now, it has been used and validated for the prediction of IDH mutant LGGs, and it has recently emerged as a non-invasive biomarker of IDH-MUT 1p/19q non co-deleted gliomas. Although the phenomenon of “T2-FLAIR suppression” was previously noted in

protoplasmic astrocytomas [66], in their pioneering study, Patel et al. described a positive correlation between the T2/FLAIR mismatch sign and the absence of 1p/19q co-deletion in IDH mutant LGGs [67]. After this study, many others reported this sign related to IDH mutation, but applied "relaxed" diagnostic criteria compared with earlier studies (i.e., heterogeneous signal on T2-weighted imaging, incomplete "suppression" on FLAIR, contrast-enhancing gliomas) [68]. This led to "false-positive" cases (all oligodendrogliomas) and failed to achieve the 100% specificity/PPV for diagnosing. In our study, we applied Patel's criteria and did not have false-positive cases. Even though the applicability of this sign seems to be limited to grade 2 and 3 gliomas, it constitutes a highly specific imaging biomarker for the IDH-MUT 1p/19q non co-deleted molecular subtype [65,67-70].
The microstructural differences in IDH-mutant 1p/19q non co-deleted astrocytomas, which are reflected in the mismatch sign, have been seldom described till now. However, the tumor matrix corresponding to the core of the mismatch sign contained numerous microcysts, which contrasted with the abundant neuroglial fibrils and cellularity in Rim [71].

Together with T2/Flair mismatch sign, the ADCm measure was the other parameter able to differentiate IDH-MUT from IDH-WT tumours. Indeed, both the ADCm and rADCm values in the mutate group were significantly higher than those of the wild type. These results strengthen the recent literature [41,61]. After the 2016 WHO brain tumour classification update, some studies investigated the role of MRI and DWI in predicting the IDH mutational status in gliomas [40,41,72–75]. In particular, our results supported the hypothesis that there are significant differences between IDH-MUT and IDH-WT tumors in terms of ultrastructural features that ADC can detect. Furthermore, we identified a "cut-off" value of ADCm $\geq 0.99 \times 10{-}3$ mm2/s (or rADCm of 1.44), which can be easily applied to differentiate the mutational status with high sensitivity and specificity. Indeed, all IDH-WT

patients had ADCm values < 0.99 × 10−3 mm2/s, with no overlaps with the IDH-MUT group.

However, ADC alone cannot differentiate IDH-WT from IDH-MUT 1p/19q co-deleted tumors since these two groups demonstrated similar ADC range values.

Indeed, ADC values might distinguish between the intact IDH-MUT group gliomas, which show significantly higher values than the IDH-MUT 1p/19q co-deleted and IDH-WT. However, IDH1-mutant 1p/19q-codeleted has frequently mixed/restricted diffusion characteristics, proving challenging to separate from IDH-WT [57].

Moreover, the ADC has been shown to correlate with prognosis and treatment responses in patients with high-grade gliomas. In particular, a low pre-treatment ADC value predicts a less favourable prognosis than higher values [76,77].

Lastly, based on classification and regression tree (CART) analysis, our proposed algorithm has given promising results. In particular, by using this classification method (a step-by-step assessment of the T2–FLAIR mismatch sign, ADC and T2W signal) the three mutational groups can be predicted with a good accuracy *(0.76),* which significantly increase *(0.89)* if we consider only gliomas of astrocytic origin. In other words, it might constitute a robust tool to help radiologists identify this group of pathologies.

Limitations

Our study has some limitations that need to be acknowledged:

-First of all the WHO classification used. Indeed, the study was developed and the data collected when the 2016 WHO classification was used, hence with the new classification scheme published in 2021 some of the included tumours would be classified differently (some IDH-WT would have been classified as GBM).

-Regarding morphological MRI features, we defined as "peritumoral edema" the T2/Flair hyper-intensity adjacent to the tumour; although commonly used, this definition might, in some cases, be inaccurate, indeed areas of white matter infiltration might have the same signal intensity of edema. However, since with conventional MRI it still remains a challenge to differentiate between these two entities, we assumed that "peritumoral edema" was predominant at the visual inspection.

-The retrospective and multi-centric nature of the study which didn't permit collecting images with homogeneous protocols.

-Concerning ADC measurement, the manual placement of ROIs could be considered another limit of our study, even if it was performed by a neuroradiologist with more than fifteen years of experience in the field of glioma MR imaging. Similarly, we have calculated rADCm values considering a normal-appearing region on T2w and contrast-enhanced T1w sequences. Furthermore, a statistical correlation between the OS of the included patients and any comorbid conditions is lacking. However, as mentioned above, the IDH-MUT patients were basically younger than the IDH-WT ones. This could be in favour of longer survival, regardless of the mutational status. Moreover, the simplified description of the diffusion process assumed in DWI sequences does not permit to completely map the complexity underlying cellular components and structures, which hinder and restrict the diffusion of water molecules. Thus, the use of more advanced MRI pulse sequences and a higher order of diffusion model (for example, through the use of multiple b values for diffusion kurtosis imaging analyses) may partially overcome these limits at the cost of less user-friendly and more time-consuming pre- and post-processing workflows.

-Considering the statistics methods used, since the performance of a model can be overestimated when determined on the sample of subjects that was used to construct it, the performance of our model can be in future studies

further assessed, in particular by applying it to an independent sample or with other models such a "leave one out" approach.

Conclusion

The association between various tumour molecular subtypes and cMRI findings provides a new opportunity for the non-invasive prediction of molecular genetics in gliomas. This association is proving to form an essential basis for preoperative, personalised surgical treatment based on molecular pathology.

In our study, cMRI demonstrated an optimal diagnostic performance for imaging prediction of IDH mutations, particularly regarding T2/FLAIR mismatch sign. Moreover, DWI is routinely performed in every MRI protocol to assess brain tumours, and our results corroborate the utility of this simple imaging biomarker for radiogenomics correlation.

Adding quantitative data such as the evaluation of ADC values to cMRI could be used routinely as an easy, non-invasive marker of specific molecular patterns and could help the decision-making process in patients with glioma. Combining the T2/FLAIR mismatch sign with the ADC parameters can improve the identification of IDH-MUT 1p/19q non co-deleted diffuse lower-grade gliomas. Moreover, imaging predictions of IDH mutations will become valued as IDH-mutant inhibitors develop clinically for neoadjuvant therapy. Lastly, prospective studies with larger patient samples, must confirm these results and validate this method. In particular adding other tumours (e.g. CNS lymphomas) which could have tissue characterised by areas or relative decrease of the diffusion coefficient could be interesting and would add a dimension of the complexity of using MRI metrics in the prediction of molecular and histological characteristics of tumours.

References

1. Louis DN, Perry A, Reifenberger G, von Deimling A, Figarella-Branger D, Cavenee WK, et al (2016) The 2016 World Health Organization Classification of Tumors of the Central Nervous System: a summary. Acta Neuropathol. 131:803-20.
2. Louis DN, Perry A, Wesseling P, Brat DJ, Cree IA, Figarella-Branger D, et al (2021) The 2021 WHO Classification of Tumors of the Central Nervous System: a summary. Neuro Oncol 23:1231-1251.
3. Hartmann, C.; Hentschel, B.; Wick, W.; Capper, D.; Felsberg, J.; Simon, M.; Westphal, M.; Schackert, G.; Meyermann, R.; Reifenberger, G.; et al. Patients with IDH1 wild type anaplastic astrocytomas exhibit worse prognosis than IDH1-mutated glioblastomas, and IDH1 mutation status accounts for the unfavorable prognostic e↵ect of higher age: Implications for classification of gliomas. *Acta Neuropathol.* **2010**, *120*, 707–718.
4. Beiko, J.; Suki, D.; Hess, K.R.; Fox, B.D.; Cheung, V.; Cabral, M.; Shonka, N.; Gilbert, M.R.; Sawaya, R.; Weinberg, J.; et al. IDH1 mutant malignant astrocytomas are more amenable to surgical resection and have a survival benefit associated with maximal surgical resection. *Neuro Oncol.* **2014**, *16*, 81–91.
5. Habib A, Jovanovich N, Hoppe M, Ak M, Mamindla P, R Colen R, Zinn PO (2021) MRI-Based Radiomics and Radiogenomics in the Management of Low-Grade Gliomas: Evaluating the Evidence for a Paradigm Shift. J Clin Med1;10:1411.
6. Bhandari A, Sharma C, Ibrahim M, Riggs M, Jones R, Lasocki A (2021) The role of 2-hydroxyglutarate magnetic resonance spectroscopy for the determination of isocitrate dehydrogenase status in lower grade gliomas versus glioblastoma: a systematic review and meta-analysis of diagnostic test accuracy. Neuroradiology 63:1823-1830.https://doi: 10.1007/s00234-021-02702-1.
7. Lu J, Li X, Li H. (2021) Perfusion parameters derived from MRI for preoperative prediction of IDH mutation and MGMT promoter methylation status in glioblastomas. Magn Reson Imaging 83:189-195.
8. Thust SC, Heiland S, Falini A, Jäger HR, Waldman AD, Sundgren PC, et al (2018) Glioma imaging in Europe: A survey of 220 centres and recommendations for best clinical practice. Eur Radiol 28:3306-3317. https://doi:10.1007/s00330-018-5314-5.
9. Le Bihan, D. Looking into the functional architecture of the brain with diffusion MRI. Nat. Rev. Neurosci. 2003, 4, 469–480.
10. Surov, A.; Meyer, H.J.; Wienke, A. Correlation between apparent diffusion coefficient (ADC) and cellularity is di↵erent in several tumors: A meta-analysis. Oncotarget 2017, 8, 59492–59499.
11. Surov, A.; Hamerla, G.; Meyer, H.J.; Winter, K.; Schob, S.; Fiedler, E. Whole lesion histogram analysis of meningiomas derived from ADC values. Correlation with several cellularity parameters, proliferation index KI 67, nucleic content

12. Kickingereder, P.; Sahm, F.; Radbruch, A.; Wick, W.; Heiland, S.; Von Deimling, A.; Bendszus, M.; Wiestler, B. IDH mutation status is associated with a distinct hypoxia/angiogenesis transcriptome signature which is non-invasively predictable with rCBV imaging in human glioma. Sci. Rep. 2015, 5, 16238.
13. Seok, J.; Yoon, S.H.; Lee, S.H.; Jung, J.H.; Lee, Y.M. The oncometabolite d-2-hydroxyglutarate induces angiogenic activity through the vascular endothelial growth factor receptor 2 signaling pathway. Int. J. Oncol. 2019, 54, 753–763.
14. Wu, H.; Tong, H.; Du, X.; Guo, H.; Ma, Q.; Zhang, Y.; Zhou, X.; Liu, H.; Wang, S.; Zhang,W.; et al. Vascular habitat analysis based on dynamic susceptibility contrast perfusion MRI predicts IDH mutation status and prognosis in high-grade gliomas. Eur. Radiol. 2020.
15. Brat DJ, Aldape K, Colman H, Holland EC, Louis DN, Jenkins RB, et al, (2018) cIMPACT-NOW update 3: recommended diagnostic criteria for "Diffuse astrocytic glioma, IDHwildtype, with molecular features of glioblastoma, WHO grade IV". Acta Neuropathol 136:805–810. https://doi.org/10.1007/ s00401-018-1913-0 4.
16. Tesileanu CMS, Dirven L, Wijnenga MMJ, Koekkoek JAF, Vincent A, Dubbink HJ, et al (2019) Survival of diffuse astrocytic glioma, IDH1/2-wildtype, with molecular features of glioblastoma, WHO grade IV: a confirmation of the cIMPACT-NOW criteria. Neuro-Oncology 22:515–523
17. Jenkins RB, et al, (2006) A t(1;19)(q10;p10) mediates the combined deletions of 1p and 19q and predicts a better prognosis of patients with oligodendroglioma. Cancer Res. 66:9852-9861.
18. Badur, M. G., Muthusamy, T., Parker, S. J., Ma, S., McBrayer, S. K., Cordes, T. et al. Oncogenic R132 IDH1 mutations limit NADPH for de novo lipogenesis through (D)2-hydroxyglutarate production in fibrosarcoma sells. *Cell Rep.* **25**, 1018.e4–1026.e4 (2018).
19. Hurley, J. H., Dean, A. M., Koshland, D. E. Jr. & Stroud, R. M. Catalytic mechanism of NADP(+)-dependent isocitrate dehydrogenase: implications from the structures of magnesium-isocitrate and NADP+ complexes. *Biochemistry* **30**, 8671–8678 (1991).
20. Han, S., Liu, Y., Cai, S.J. *et al.* IDH mutation in glioma: molecular mechanisms and potential therapeutic targets. *Br J Cancer* **122,** 1580–1589 (2020).
21. Jalbert, L.E.; Elkhaled, A.; Phillips, J.J.; Neill, E.; Williams, A.; Crane, J.C.; Olson, M.P.; Molinaro, A.M.; Berger, M.S.; Ronen, S.M.; et al. Metabolic profiling of IDH mutation and malignant progression in infiltrating glioma. Sci. Rep. 2017, 7, 44792.
22. Sanson, M.; Marie, Y.; Paris, S.; Idbaih, A.; Laffaire, J.; Ducray, F.; El Hallani, S.; Boisselier, B.; Mokhtari, K.; Delattre, J.Y.; et al. Isocitrate dehydrogenase 1 codon 132 mutation is an important prognostic biomarker in gliomas. J. Clin. Oncol. 2009, 27, 4150–4154.
23. Yan, H.; Parsons, D.W.; Jin, G.; McLendon, R.; Rasheed, B.A.; Yuan,W.; Kos, I.; Batinic-Haberle, I.; Jones, S.; Friedman, H.; et al. IDH1 and IDH2 mutations in gliomas. N. Engl. J. Med. 2009, 360, 765–773.

24. Watanabe, T.; Nobusawa, S.; Kleihues, P.; Ohgaki, H. IDH1 mutations are early events in the development of astrocytomas and oligodendrogliomas. Am. J. Pathol. 2009, 174, 1149–1153.
25. Hartmann, C.; Meyer, J.; Balss, J.; Capper, D.; Mueller, W.; Christians, A.; Felsberg, J.; Wolter, M.; Mawrin, C.; Weller, M.; et al. Type and frequency of IDH1 and IDH2 mutations are related to astrocytic and oligodendroglial dfferentiation and age: A study of 1,010 diffuse gliomas. Acta Neuropathol. 2009, 118, 469–474.
26. Camelo-Piragua S, et al (2010) Mutant IDH1-specific immunohistochemistry distinguishes diffuse astrocytoma from astrocytosis. Acta Neuropathol. 119:509-511.
27. Horbinski C, et al. (2009) Diagnostic use of IDH1/2 mutation analysis in routine clinical testing of formalin-fixed, paraffin-embedded glioma tissues. J Neuropathol Exp Neurol. 68:1319-1325.
28. Leu K, Ott GA, Lai A, et al. Perfusion and diffusion MRI signatures in histologic and genetic subtypes of WHO grade II-III diffuse gliomas. J Neurooncol 2017;134:177–188
29. Sehgal V, Delproposto Z, Haacke EM, et al. Clinical applications of neuroimaging with susceptibilityweighted imaging. J Magn Reson Imaging 2005;22:439–450.
30. Zhang W, Zhao J, Guo D, et al. Application of susceptibility weighted imaging in revealing intratumoral blood products and grading gliomas. J Radiol 2010;91:485–490.
31. Iima M, Le Bihan D. Clinical Intravoxel Incoherent Motion and Diffusion MR Imaging: Past, Present, and Future. Radiology. 2016;278:13–32.
32. Dietrich O, Biffar A, Baur-Melnyk A, Reiser MF. Technical aspects of MR diffusion imaging of the body. Eur J Radiol. 2010;76:314–322.
33. Einstein A. On the movement of small particles suspended in stationary liquids required by the kinetic theory of heat. Ann Der Physik. 1905;17:549–560.
34. Kwee TC, Takahara T, Ochiai R, Katahira K, Van Cauteren M, Imai Y, Nievelstein RA, Luijten PR. Whole-body diffusion-weighted magnetic resonance imaging. Eur J Radiol. 2009;70:409–417.
35. Stejskal EO, Tanner JE. Spin diffusion measurements: spin echoes in the presence of a time-dependent field gradient. J Chem Phys 1965;42:288–92.
36. Benz MR, Vargas HA, Sala E. Functional MR Imaging Techniques in Oncology in the Era of Personalized Medicine. Magn Reson Imaging Clin N Am. 2016;24:1-10.
37. Kono K., et al. The role of diffusion-weighted imaging in patients with brain tumors. AJNR Am J Neuroradiol. 2001;22:1081108-8.
38. Padhani AR, Koh DM, Collins DJ. Whole-body diffusion-weighted MR imaging in cancer: current status and research directions. Radiology. 2011;261:700–718.
39. Liu, T.; Cheng, G.; Kang, X.; Xi, Y.; Zhu, Y.; Wang, K.; Sun, C.; Ye, J.; Li, P.; Yin, H. Noninvasively evaluating the grading and IDH1 mutation status of diffuse gliomas by three-dimensional pseudo-continuous arterial spin labeling and diffusion-weighted imaging. *Neuroradiology* **2018**, *60*, 693–702.

40. Xing, Z.; Yang, X.; She, D.; Lin, Y.; Zhang, Y.; Cao, D. Noninvasive Assessment of IDH Mutational Status in World Health Organization Grade II and III Astrocytomas Using DWI and DSC-PWI Combined with Conventional MR Imaging. *AJNR Am. J. Neuroradiol.* **2017**, *38*, 1138–1144.
41. Shboul, Z.A.; Chen, J.; Miftekharuddin, K. Prediction of Molecular Mutations in Diffuse Low-Grade Gliomas using MR Imaging Features. *Sci. Rep.* **2020**, *10*, 3711.
42. Delfanti, R.L.; Piccioni, D.E.; Handwerker, J.; Bahrami, N.; Krishnan, A.; Karunamuni, R.; Snyder, V.S. Imaging Correlates for the 2016 Update on WHO Classification of Grade II/III Gliomas: Implications for IDH, 1p/19q and ATRX Status. *J. Neuro-Oncol.* **2017**, *135*, 601–609.
43. Bulakbas ı, N.; Paksoy, Y. Advanced imaging in adult diffusely infiltrating low-grade gliomas. *Insights Imaging* **2019**, *10*, 122.
44. Hu, Y.C.; Yan, L.F.; Sun, Q.; Liu, Z.C.; Wang, S.M.; Han, Y.; Tian, Q.; Sun, Y.Z.; Zheng, D.D.; Cui, G.B.; et al. Comparison between ultra-high and conventional mono b-value DWI for preoperative glioma grading. *Oncotarget* **2017**, *8*, 37884–37895.
45. Wang, Q.P.; Lei, D.Q.; Yuan, Y.; Xiong, N.X. Accuracy of ADC derived from DWI for differentiating high-grade from low-grade gliomas: Systematic review and meta-analysis. *Medicine* **2020**, *99*, e19254.
46. Tan, Y.; Zhang, H.; Wang, X.C.; Qin, J.B.; Wang, L. The value of multi ultra high-b-value DWI in grading cerebral astrocytomas and its association with aquaporin-4. *Br. J. Radiol.* **2018**, *91*, 20170696.
47. Chen, S.D.; Hou, P.F.; Lou, L.; Jin, X.; Wang, T.H.; Xu, J.L. The correlation between MR diffusion-weighted imaging and pathological grades on glioma. *Eur. Rev. Med. Pharmacol. Sci.* **2014**, *18*, 1904–1909.
48. Van Den Bent, M.J.; Hartmann, C.; Preusser, M.; Str bel, T.; Dubbink, H.J.; Kros, J.M.; von Deimling, A.; Boisselier, B.; Sanson, M.; Diefes, K.L.; et al. Interlaboratory comparison of IDH mutation detection. J. Neuro-Oncol. 2013, 112, 173–178.
49. Horbinski, C.; Miller, C.R.; Perry, A. Gone FISHing: Clinical lessons learned in brain tumor molecular diagnostics over the last decade. Brain Pathol. 2011, 21, 57–73.
50. R Core Team (2014). R: A language and environment for statistical computing. R Foundation for Statistical Computing, Vienna, Austria. URL http://www.R-project.org/.
51. Tang Q, Lian Y, Yu J, Wang Y, Shi Z, Chen L (2017) Anatomic mapping of molecular subtypes in diffuse glioma. BMC Neurol 15;17:183. https://doi: 10.1186/s12883-017-0961-8.
52. Darlix A, Deverdun J, Menjot de Champfleur N, Castan F, Zouaoui S, Rigau V et al (2017) IDH mutation and 1p19q codeletion distinguish two radiological patterns of diffuse low-grade gliomas. J Neurooncol 133:37-45. https:doi: 10.1007/s11060-017-2421-0.
53. Zhao K, Sun G, Wang Q, Xue Z, Liu G, Xia Y, et al (2020) The Diagnostic Value of Conventional MRI and CT Features in the Identification of the IDH1-Mutant

and 1p/19q Co-Deletion in WHO Grade II Gliomas. Acad Radiol 28:S1076-6332(20)30149-5. https://doi: 10.1016/j.acra.2020.03.008.
54. Park YW, Han K, Ahn SS, Bae S, Choi YS, Chang JH, et al (2018) Prediction of IDH1-Mutation and 1p/19q-Codeletion Status Using Preoperative MR Imaging Phenotypes in Lower Grade Gliomas
55. Kim JW, Park CK, Park SH, et al. Relationship between radiological characteristics and combined 1p and 19q deletion in World Health Organization grade III oligodendroglial tumours. J Neurol Neurosurg Psychiatry. 2011;82(2):224–227.
56. Kern M, Auer TA, Picht, T. et al (2020) T2 mapping of molecular subtypes of WHO grade II/III gliomas. BMC Neurol 20, 8. AJNR Am J Neuroradiol 39:37-42. https://doi: 10.3174/ajnr.A5421.
57. Smits M (2020) Imaging of oligodendroglioma. Br J Radiol 89:20150857.https://doi:10.1259/bjr.20150857.
58. Kong LW, Chen J, Zhao H, Yao K, Fang SY, Wang Z, Wang YY, Li SW (2019) Intratumoral Susceptibility Signals Reflect Biomarker Status in Gliomas. Sci Rep 9:17080. https://doi: 10.1038/s41598-019-53629-w.
59. Castet F, Alanya E, Vidal N, Izquierdo C, Mesia C, Ducray F, et al (2019) Contrast-enhancement in supratentorial low-grade gliomas: a classic prognostic factor in the molecular age. J Neurooncol 143:515-523.
60. Yamauchi T, Ohno M, Matsushita Y, et al. Radiological characteristics based on isocitrate dehydrogenase mutations and 1p/19q codeletion in grade II and III gliomas. Brain Tumor Pathol. 2018;35(3):148–158.
61. Feraco P, Bacci A, Ferrazza P, van den Hauwe L, Pertile R, Girlando S, et al (2020) Magnetic Resonance imaging Derived Biomarkers of IDH Mutation Status and Overall Survival in Grade III Astrocytomas. B.Diagnostics (Basel) 10:247. https://doi: 10.3390/diagnostics10040247.
62. Qi S, Yu L, Li H, et al. Isocitrate dehydrogenase mutation is associated with tumor location and magnetic resonance imaging characteristics in astrocytic neoplasms. Oncol Lett. 2014;7(6):1895–1902.
63. Hempel JM, Brendle C, Bender B, Bier G, Skardelly M, Gepfner-Tuma I, et al (2018) Schittenhelm. Contrast enhancement predicting survival in integrated molecular subtypes of diffuse glioma: an observational cohort study. J Neurooncol 139:373-381. https://doi:10.1007/s11060-018-2872-y.
64. Zhou H, Vallières M, Bai HX, Su C, Tang H, Oldridge D et al (2017) MRI features predict survival and molecular markers in diffuse lower-grade gliomas. Neuro Oncol 19:862-870.
65. Foltyn M, Nieto Taborda KN, Neuberger U, Brugnara G, Reinhardt A, Stichel D, et al (2020) T2/FLAIR-mismatch sign for noninvasive detection of IDH-mutant 1p/19q non-codeleted gliomas: validity and pathophysiology. Neurooncol Adv 10;2:vdaa004.
66. Tay KL, Tsui A, Phal PM, Drummond KJ, Tress BM. MR imaging characteristics of protoplasmic astrocytomas. Neuroradiology. 2011;53(6):405–411.
67. Patel SH, Poisson LM, Brat DJ, Zhou Y, Cooper L, Snuderl M, et al (2017) T2-FLAIR Mismatch, an Imaging Biomarker for IDH and 1p/19q Status in Lower-

grade Gliomas: A TCGA/TCIA Project. Clin Cancer Res 23(20):6078-6085. https://doi: 10.1158/1078-0432.CCR-17-0560.
68. Jain R, Johnson DR, Patel SH, Castillo M, Smits M, van den Bent MJ, Chi AS, Cahill DP. "Real world" use of a highly reliable imaging sign: "T2-FLAIR mismatch" for identification of IDH mutant astrocytomas. Neuro Oncol. 2020 Jul 7;22(7):936-943. doi: 10.1093/neuonc/noaa041.
69. Corell A, Ferreyra Vega S, Hoefling N, Carstam L, Smits A, Olsson Bontell T, et al (2020) The clinical significance of the T2-FLAIR mismatch sign in grade II and III gliomas: a population-based study. BMC Cancer 20:450.
70. Lee MK, Park JE, Jo Y, Park SY, Kim SJ, Kim HS (2020) Advanced imaging parameters improve the prediction of diffuse lower-grade gliomas subtype, IDH mutant with no 1p19q codeletion: added value to the T2/FLAIR mismatch sign. Eur Radiol 30:844-854. https://doi: 10.1007/s00330-019-06395-2.
71. Fujita Y, Nagashima H, Tanaka K, Hashiguchi M, Hirose T, Itoh T, Sasayama T. The Histopathologic and Radiologic Features of T2-FLAIR Mismatch Sign in IDH-Mutant 1p/19q Non-codeleted Astrocytomas. World Neurosurg. 2021 May;149:e253-e260. doi: 10.1016/j.wneu.2021.02.042.
72. Thust SC, Hassanein S, Bisdas S, Rees JH, Hyare H, Maynard JA et al (2018) Apparent diffusion coefficient for molecular subtyping of non-gadolinium-enhancing WHO grade II/III glioma: volumetric segmentation versus two-dimensional region of interest analysis. Eur Radiol 28(9):3779-3788.
73. Pruis IJ, Koene SR, van der Voort SR, Incekara F, Vincent AJPE, van den Bent MJ, Lycklama À Nijeholt GJ, Nandoe Tewarie RDS, Veldhuijzen van Zanten SEM, Smits M. Noninvasive differentiation of molecular subtypes of adult nonenhancing glioma using MRI perfusion and diffusion parameters. Neurooncol Adv. 2022 Feb 21;4(1):vdac023.
74. Nuessle NC, Behling F, Tabatabai G, Castaneda Vega S, Schittenhelm J, Ernemann U, Klose U, Hempel JM. ADC-Based Stratification of Molecular Glioma Subtypes Using High b-Value Diffusion-Weighted Imaging. J Clin Med. 2021 Aug 4;10(16):3451.
75. Zhang J, Peng H, Wang YL, Xiao HF, Cui YY, Bian XB, Zhang DK, Ma L. Predictive Role of the Apparent Diffusion Coefficient and MRI Morphologic Features on IDH Status in Patients With Diffuse Glioma: A Retrospective Cross-Sectional Study. Front Oncol. 2021 May 13;11:640738.
76. Yamasaki, F.; Sugiyama, K.; Ohtaki, M.; Takeshima, Y.; Abe, N.; Akiyama, Y.; Takaba, J.; Amatya, V.J.; Saito, T.; Hanaya, R.; et al. Glioblastoma treated with postoperative radiochemotherapy: Prognostic value of apparent di↵usion coecient at MR imaging. *Eur. J. Radiol.* **2010**, *73*, 532–537.
77. Nakamura, H.; Murakami, R.; Hirai, T.; Kitajima, M.; Yamashita, Y. Can MRI-derived factors predict the survival in glioblastoma patients treated with postoperative chemoradiation therapy? *Acta Radiol.* **2013**, *54*, 214–220.